Supporting Information

Selective Oxidation of Methane to Formaldehyde Catalyzed by Phosphates: Kinetic Description by Bond strengths and Specific Total Acidities.

Vasilij Gomonaj[†] and Hervé Toulhoat[*,‡,§]

[†]National University of Uzhgorod, Department of Physical and Colloid Chemistry, Pidhirna Street, 46, Uzhgorod 380, Ukraine
[‡] IFP Energies nouvelles, 1 & 4 avenue de Bois-Préau, 92852 Rueil-Malmaison, France
[§]Sorbonne Université, UPMC Univ Paris 06, UMR CNRS 7197, Laboratoire de Réactivité de Surface, Tour 43-33, 3ème étage, Case 178, 4 Place Jussieu, F-75252, Paris, France

[*]**Corresponding Author:**
Hervé Toulhoat
Email: herve.toulhoat@orange.fr

SI-1 - Catalysts characterization

X-Ray diffraction

For catalysts $Mn_2P_2O_7$, $CrPO_4$, $Co_3(PO_4)_2$, $Ni_3(PO_4)_2$, $FePO_4$, $AlPO_4$, BPO_4 , SiP_2O_7 , Powder diffraction spectra were recorded in the $2\theta = 20\text{-}50°$ Bragg angle interval thanks to an automated DRON-UM1 diffractometer equipped with a Cobalt anticathode and an iron filter. Inter-reticular distances d_i were computed according to the Wulff-Bragg formula $n\lambda = 2d_i \sin\theta_i$ with $\lambda = 1{,}7909$ Å the Co Kα incident radiation wavelength. For catalysts TiP_2O_7, GeP_2O_7 , SnP_2O_7 , and $Mg_3(PO_4)_2$ powder diffraction spectra were recorded in the $2\theta = 10\text{-}60°$ Bragg angle interval using a more recent diffractometer equipped with a Copper anticathode ($\lambda = 1{,}5418$ Å). The diffraction peaks intensities were normalized between 0 and 100 arbitrary units.

The powder diffraction spectra were recorded on all phosphate samples firstly after drying the freshly prepared precipitates at 393 K, and secondly after calcination at 973K. Dried samples exhibited very diffuse diffraction lines, indicative of poorly crystallized or amorphous solids, while calcined phosphates exhibited thin lines with well-defined peak positions, indicative of well crystallized solids. The corresponding crystal structures were determined by comparison with tabulated reference spectra and moreover with simulated spectra as presented below. Simulations were performed thanks to the VESTA program (1) on the basis of the published reference structures as cited in the main text.

Importantly, all used catalysts were again characterized, showing no change with respect to the freshly calcined solids.

We present hereafter for each phosphate catalyst representative of a particular structure (i.e. space group): 1) experimental X Ray diffraction patterns; 2) simulated diffractions patterns for the matching reference structure; 3) a list of experimental and calculated reticular distances and the corresponding relative intensities for the main diffraction peaks; 4) the corresponding correlation diagrams between distances, with the regression line (dotted line, with equation and squared coefficient of correlation in inset).

$Mn_2P_2O_7$ C 2/m

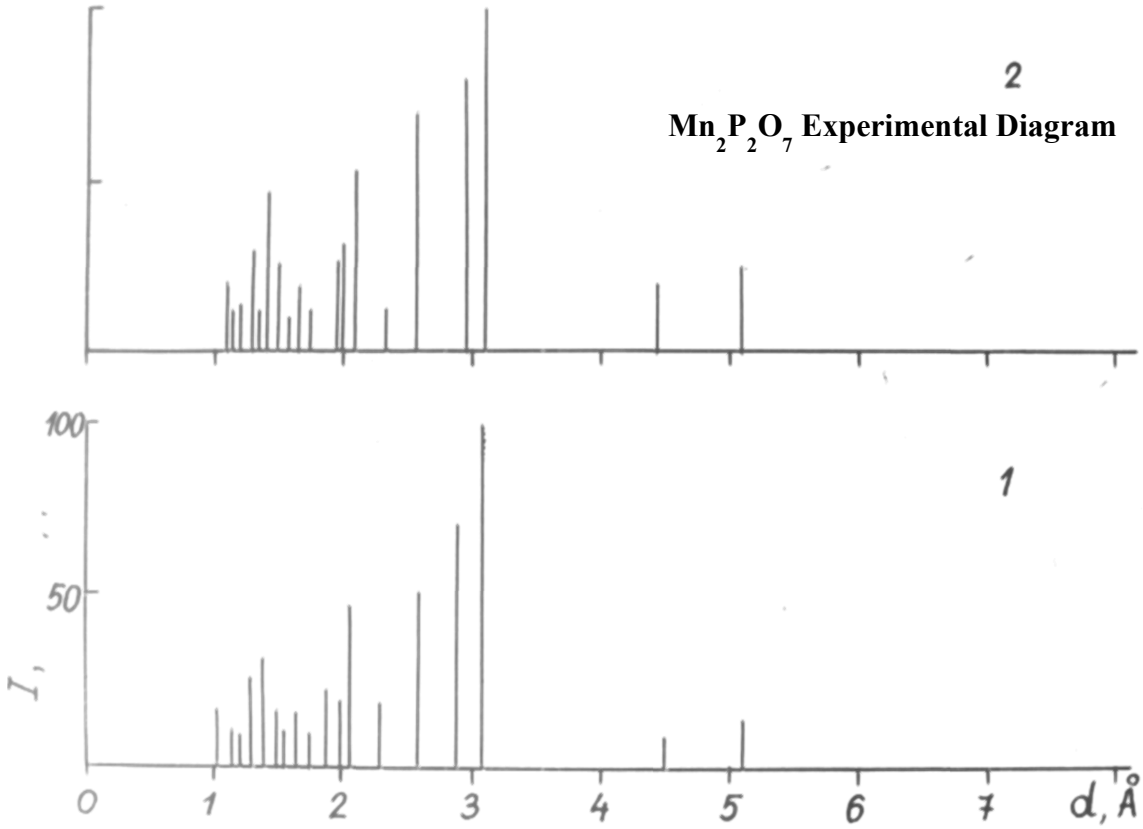

$Mn_2P_2O_7$ Experimental Diagram

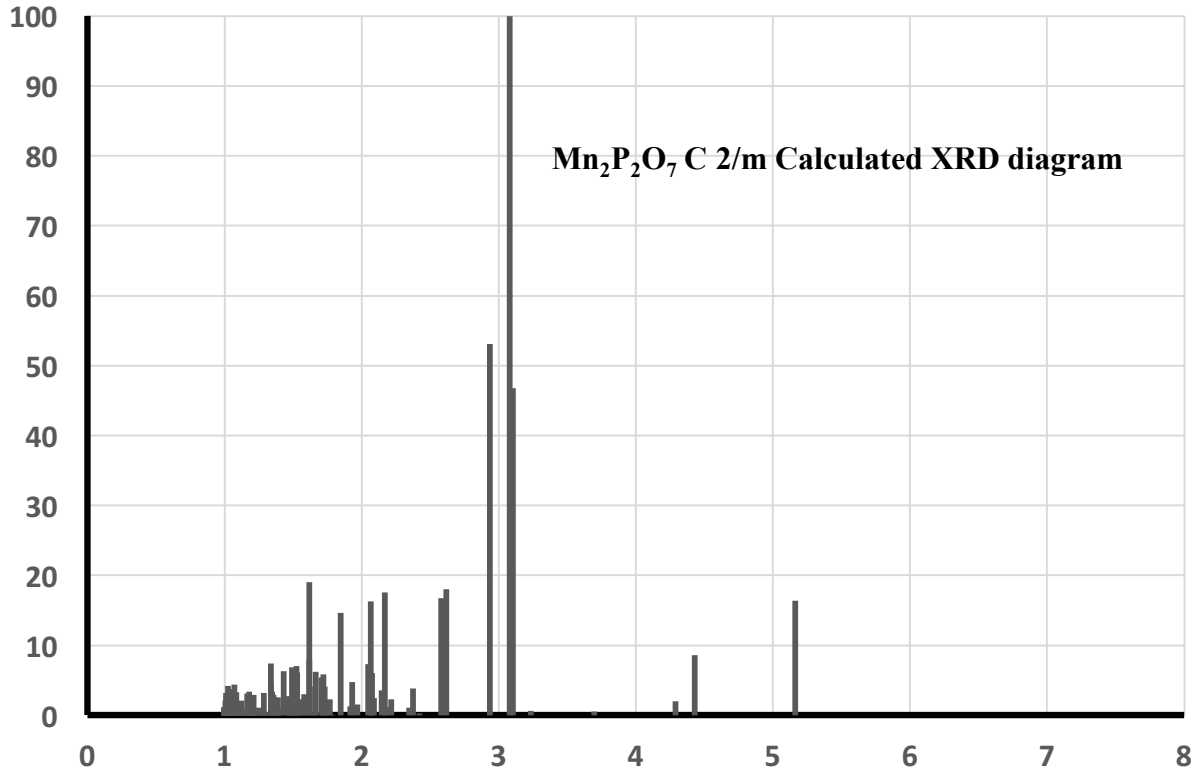

$Mn_2P_2O_7$ C 2/m Calculated XRD diagram

$Mn_2P_2O_7$
Main lines

Exp d (A°)	exp I	Calc d (A°)	Calc I
5,2	8	5,16	16
4,45	6	4,43	9
3,1	100	3,08	100
2,95	50	2,94	53
2,6	20	2,62	18
2,37	1	2,37	4
2,17	18	2,17	18
2,07	18	2,07	16
1,85	10	1,85	15

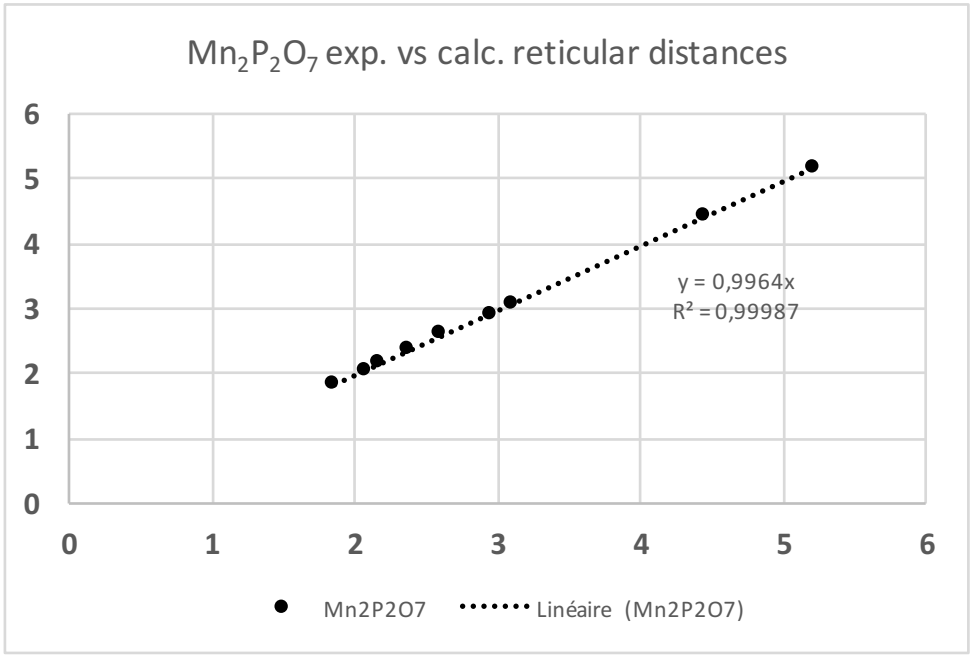

$CrPO_4$ Cmcm

$CrPO_4$ Cmcm Experimental XRD diagram

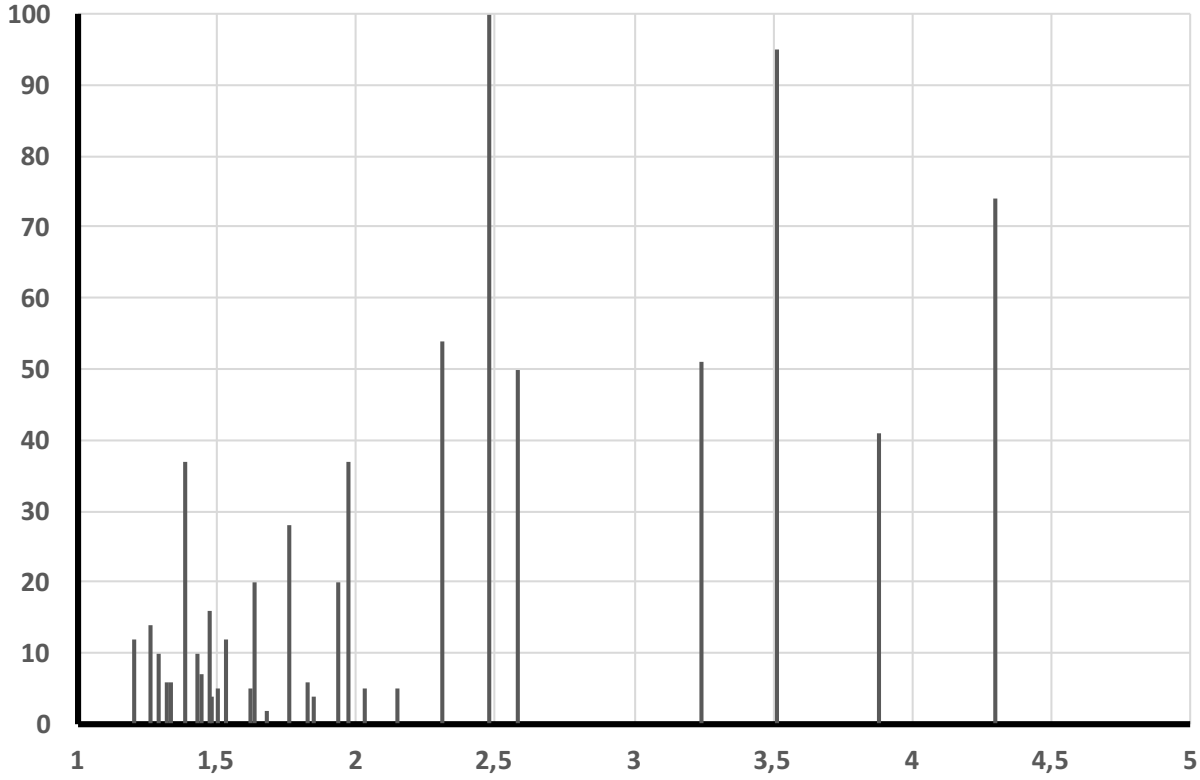

$CrPO_4$ Cmcm Calculated XRD diagram

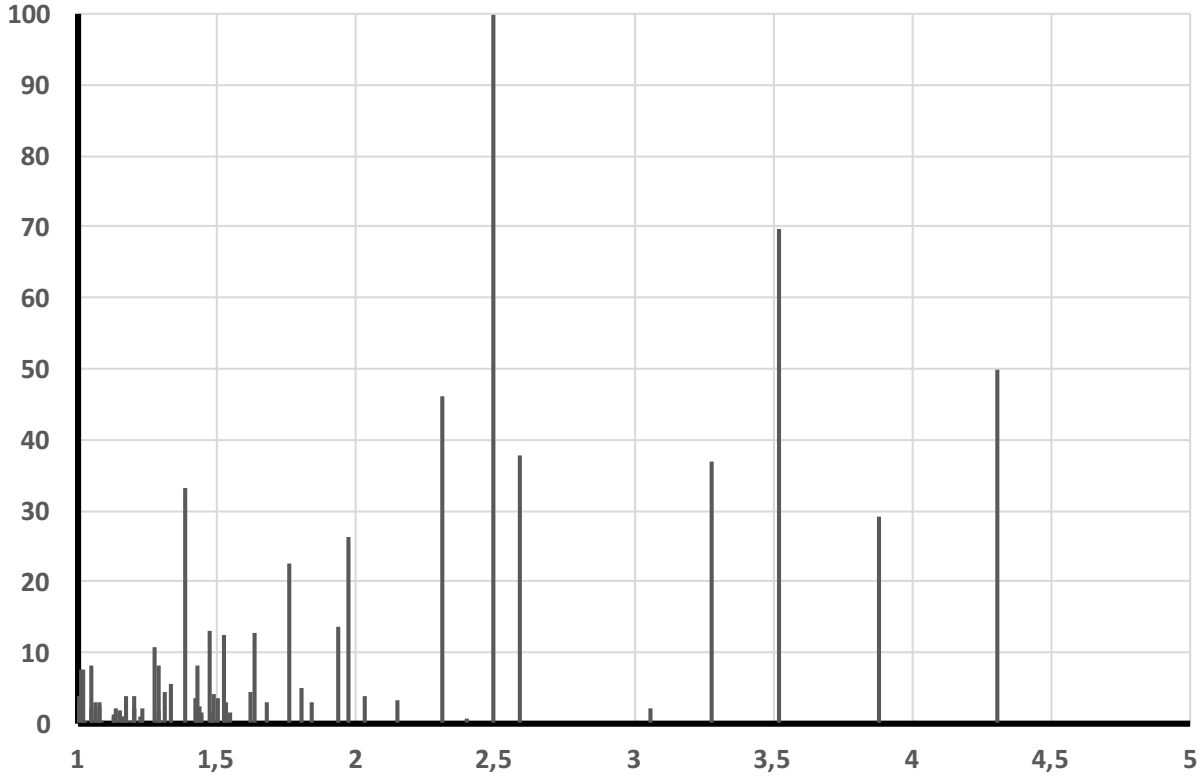

$CrPO_4$ Main lines

Exp d (A°)	exp. I	Calc. d (A°)	Calc. I
4,30	74	4,30	50
3,88	41	3,88	29
3,51	95	3,52	70
3,24	51	3,28	37
2,58	50	2,59	38
2,48	100	2,49	100
2,31	54	2,31	46
2,15	5	2,15	3
2,03	5	2,03	4
1,975	37	1,97	26
1,938	20	1,94	14
1,845	4	1,85	0
1,828	6	1,84	3
1,76	28	1,76	23
1,681	2	1,68	3
1,637	20	1,64	13
1,621	5	1,62	5
1,531	12	1,53	13
1,502	5	1,50	4
1,484	4	1,49	4
1,473	16	1,47	13
1,443	7	1,44	3
1,433	10	1,43	8
1,383	37	1,38	33
1,337	6	1,34	6
1,319	6	1,32	4
1,29	10	1,29	8
1,26	14	1,28	11
1,202	12	1,20	4

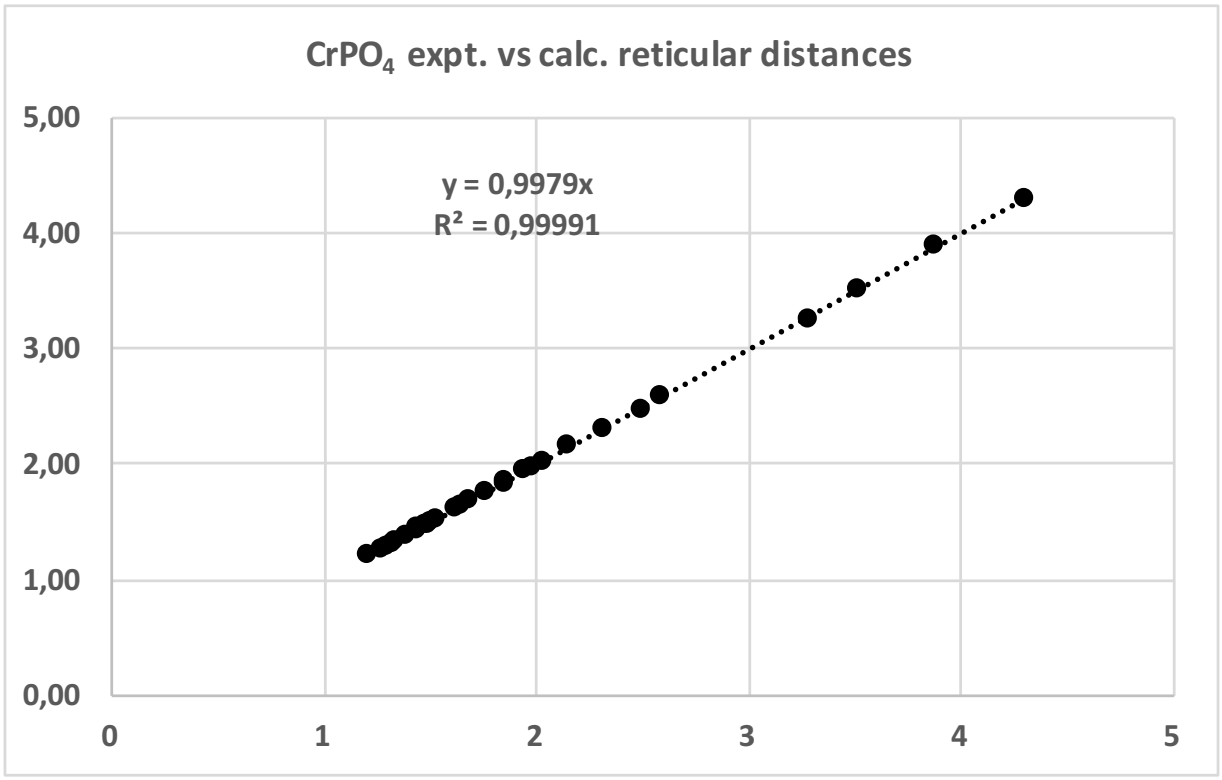
CrPO4 expt. vs calc. reticular distances
y = 0,9979x
R² = 0,99991
5,00
4,00
3,00
2,00
1,00
0,00
0
1
2
3
4
5

$Co_3(PO_4)_2$ P-1

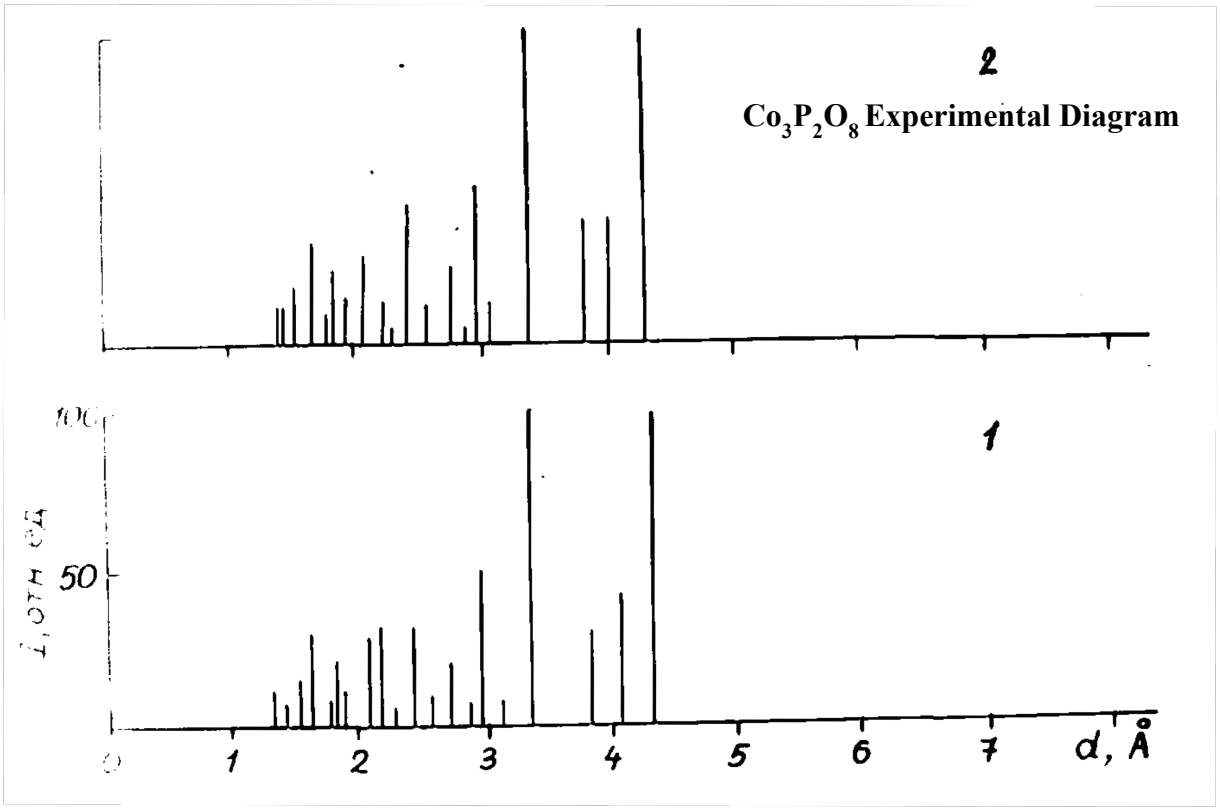
2
$Co_3P_2O_8$ Experimental Diagram
1
50
1
2
3
4
5
6
7
d, Å

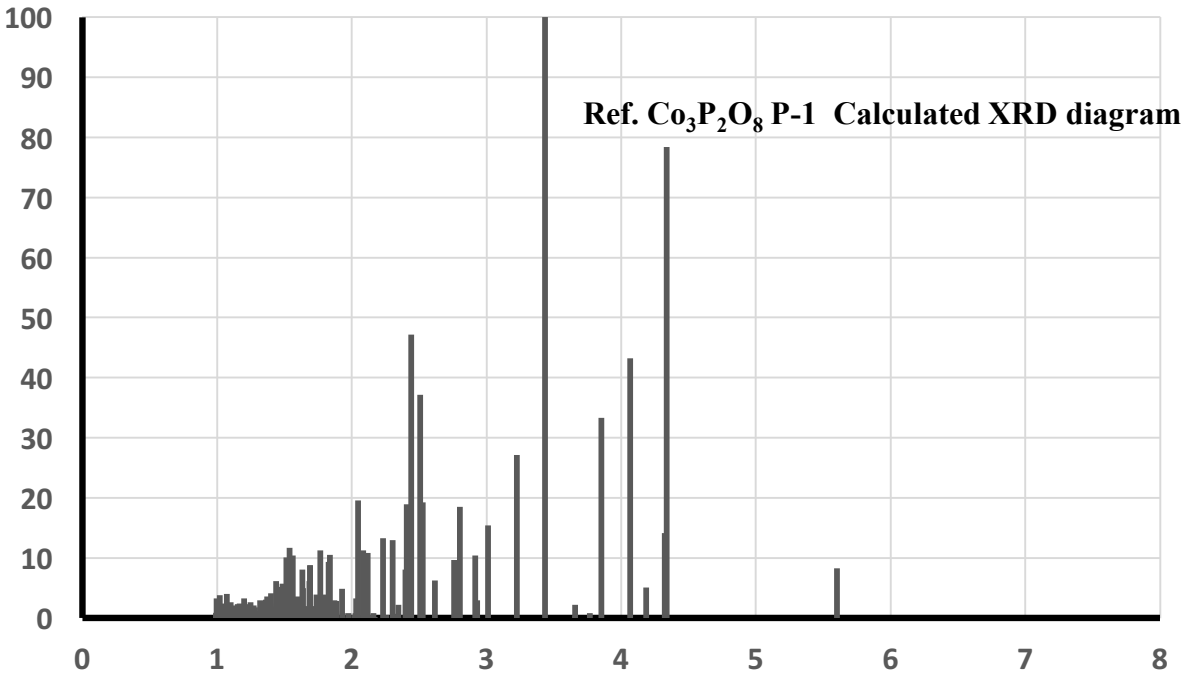
Ref. $Co_3P_2O_8$ P-1 Calculated XRD diagram
100
90
80
70
60
50
40
30
20
10
0
0
1
2
3
4
5
6
7
8

$Co_3(PO_4)_2$ Main Lines

Exp d(A°)	exp I	Calc d (A°)	Calc I
4,33	100	4,34	78
4,09	30	4,07	43
3,85	30	3,85	33
3,44	100	3,44	100
3,21	23	3,22	27
3	13	3,01	15
2,9	3	2,93	3
2,78	20	2,80	18
2,6	7	2,62	6
2,51	33	2,51	37
2,48	50	2,44	47
2,3	3	2,30	13
2,23	7	2,23	13
2,1	2	2,10	2
2,03	10	2,05	20
1,93	7	1,93	5
1,87	3	1,87	3
1,83	13	1,84	11
1,74	7	1,77	11
1,69	17	1,69	24
1,63	10	1,63	13
1,59	3	1,59	2
1,56	10	1,56	10
1,54	10	1,54	12
1,51	7	1,51	10
1,48	7	1,48	6
1,45	10	1,45	10
1,39	7	1,39	7
1,37	7	1,37	7

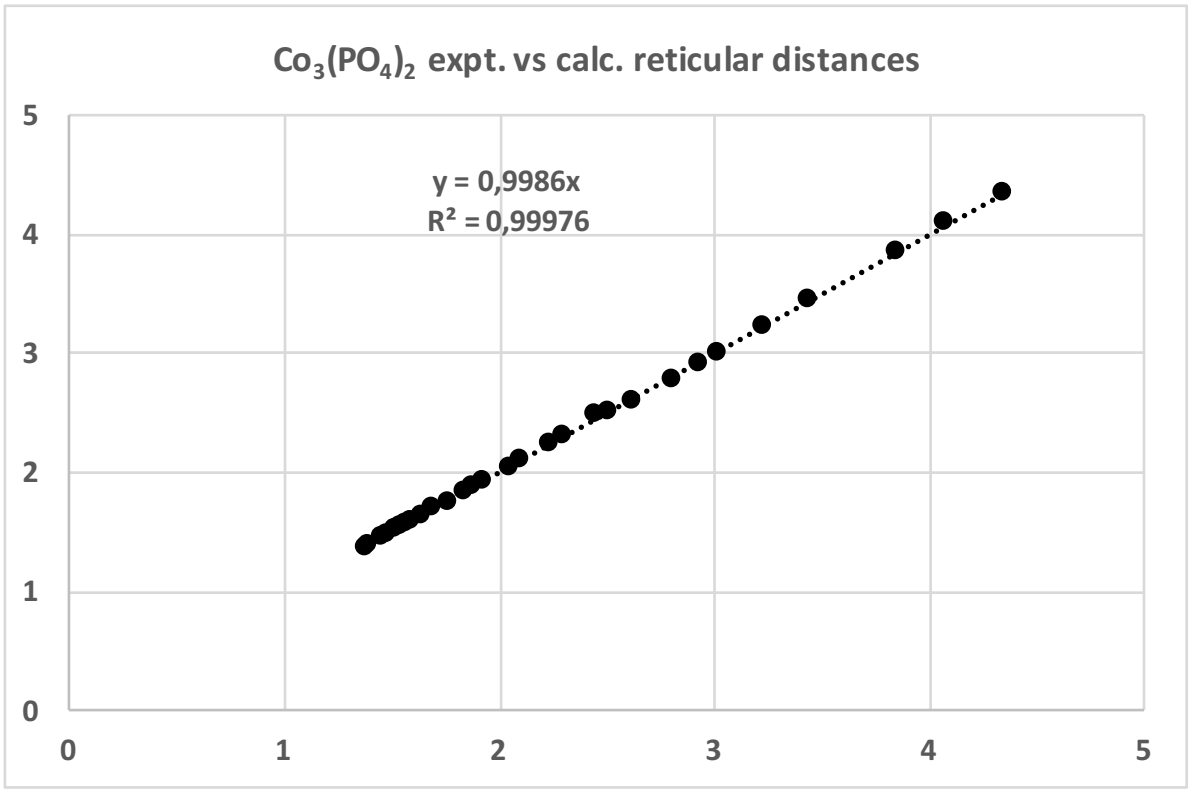
Co3(PO4)2 expt. vs calc. reticular distances
y = 0,9986x
R² = 0,99976
0
1
2
3
4
5
0
1
2
3
4
5

$Ni_3(PO_4)_2$ P1 21/a1

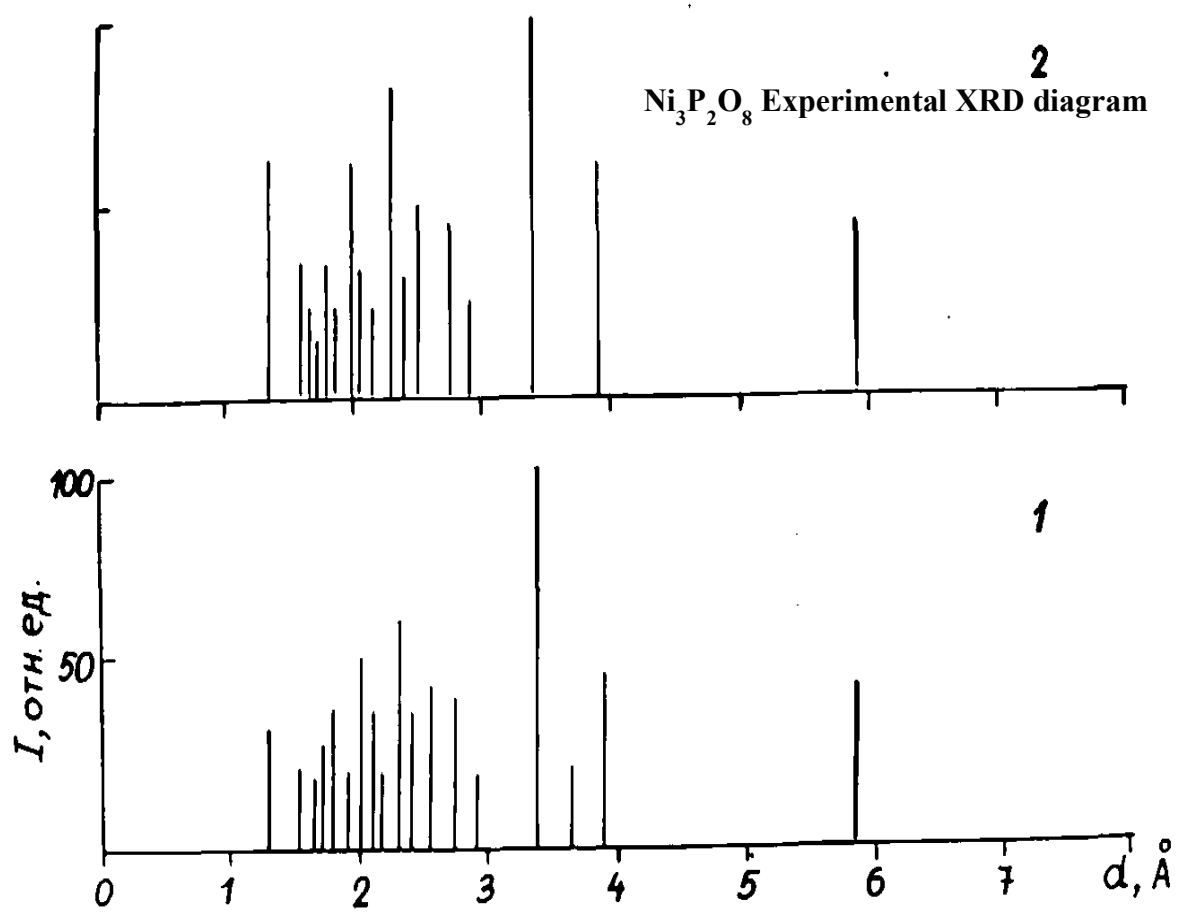

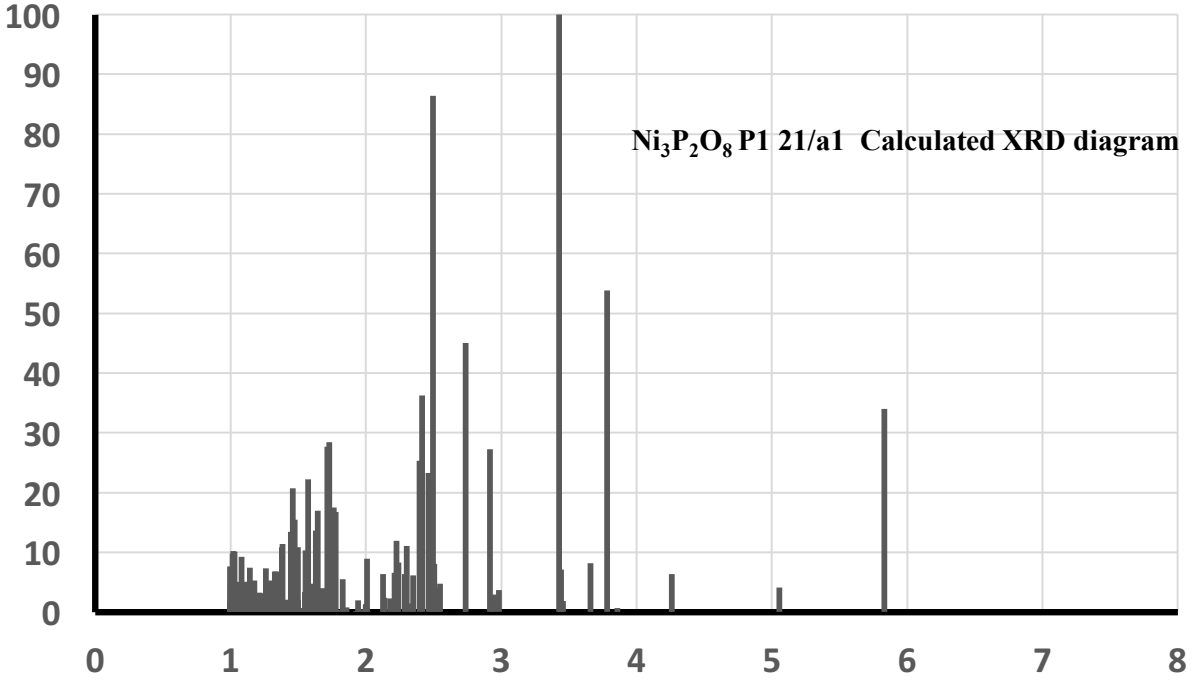

$Ni_3P_2O_8$ Main lines

Exp d(A°)	exp I	Calc d (A°)	Calc I
5,82	45	5,83	34
3,81	63	3,78	54
3,56	22	3,66	8
3,34	100	3,43	100
2,82	24	2,91	27
2,68	46	2,74	45
2,45	51	2,49	86
2,30	33	2,30	11
2,24	83	2,23	12

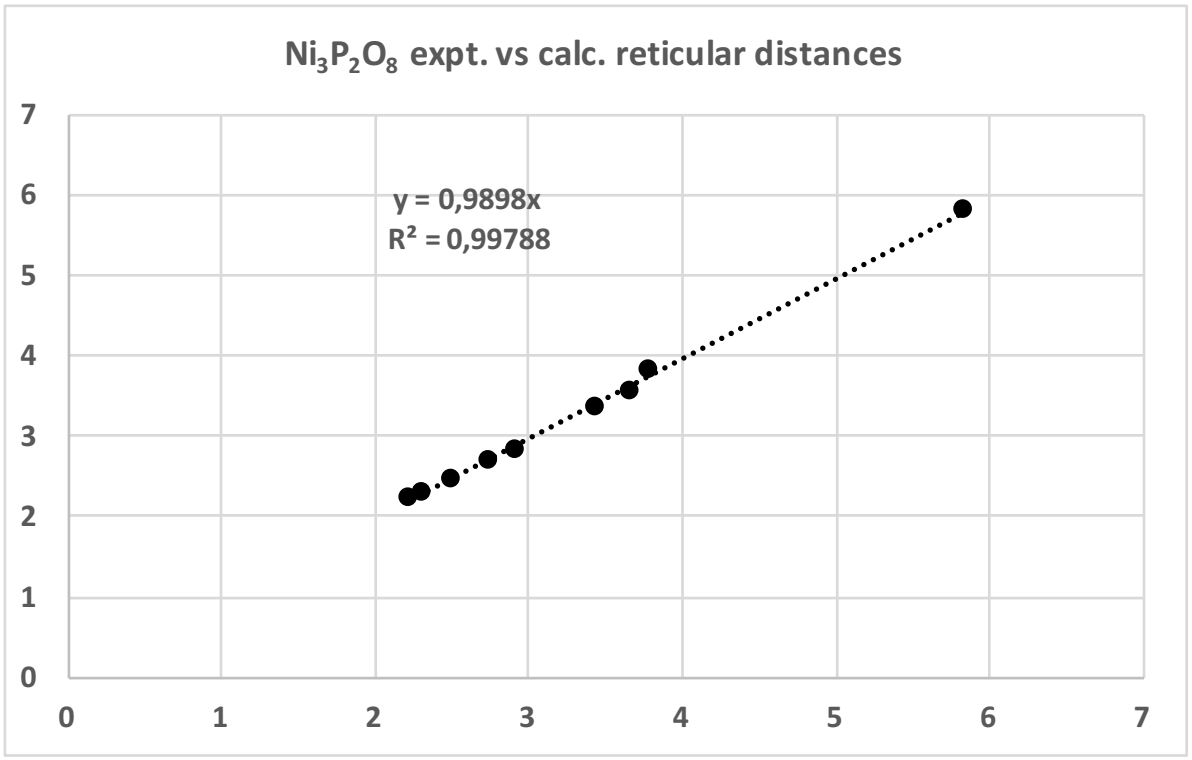

$FePO_4$ P3121

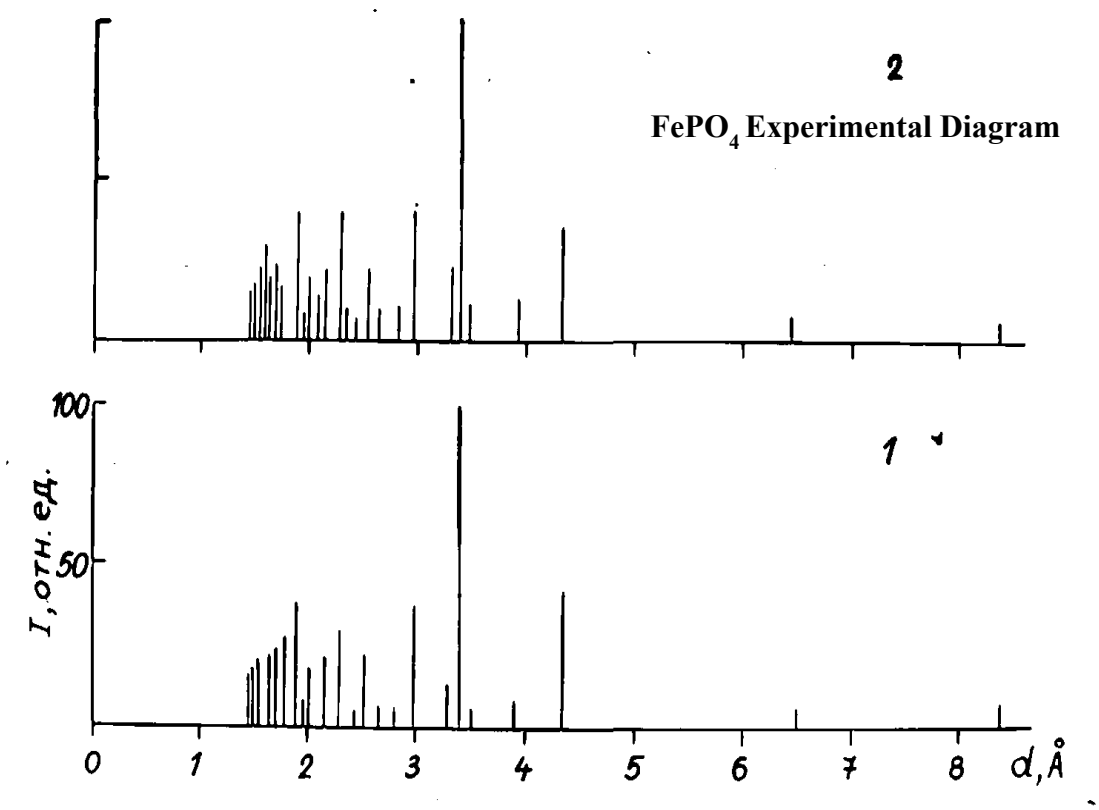

$FePO_4$ Experimental Diagram

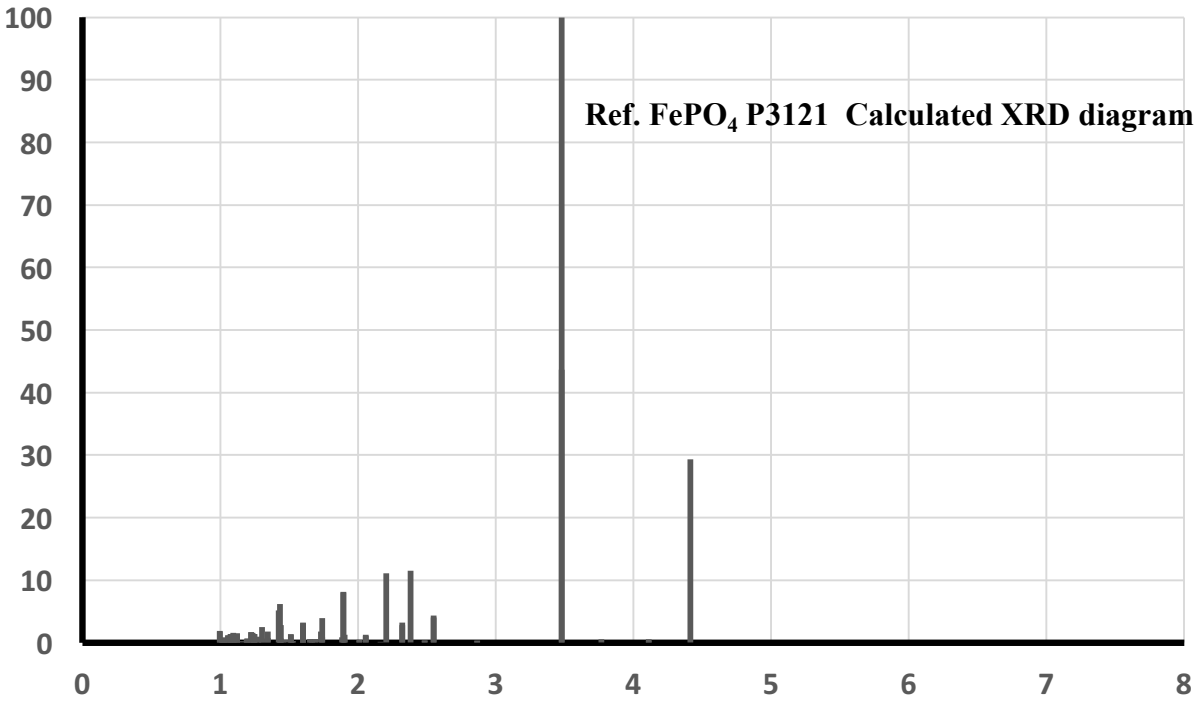

Ref. $FePO_4$ P3121 Calculated XRD diagram

$FePO_4$ Main lines

Exp d(A°)	exp I	Calc d (A°)	Calc I
4,31	45	4,42	29,3
3,85	9,6	3,77	0,6
3,49	6,2	3,48	43,6
3,35	100	3,48	100,0
2,95	41,4	2,87	0,5
1,905	36	1,89	16,0

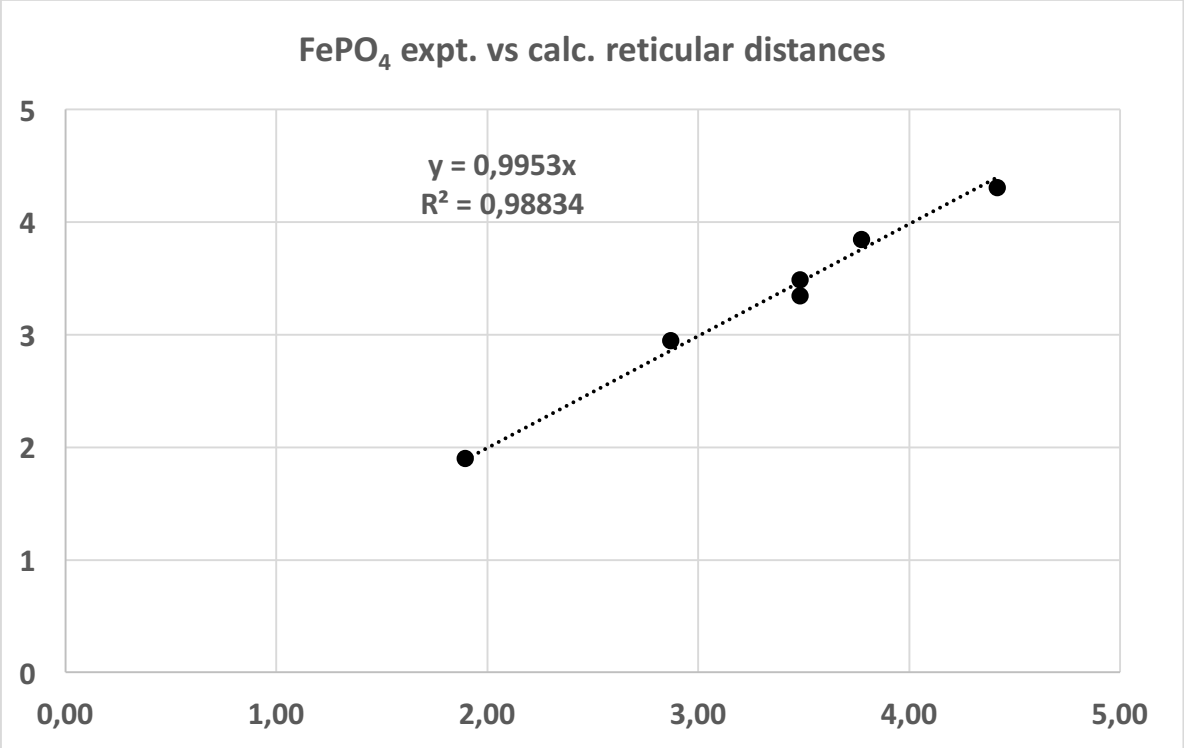

$Mg_3(PO_4)_2$ P2_1/c

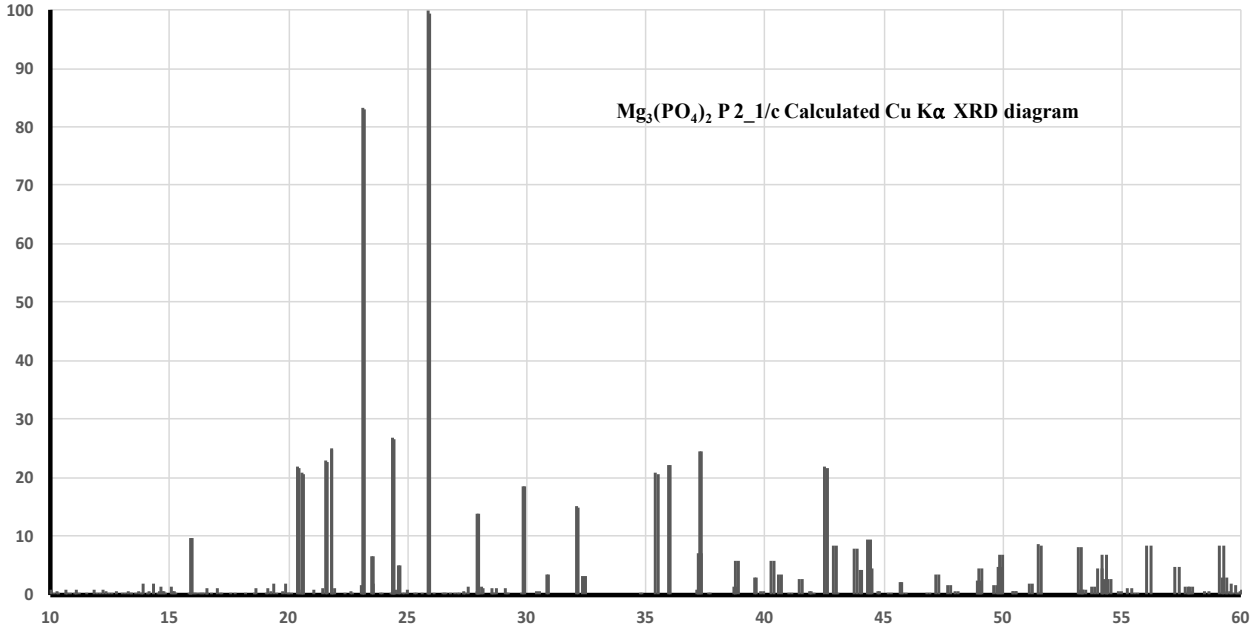

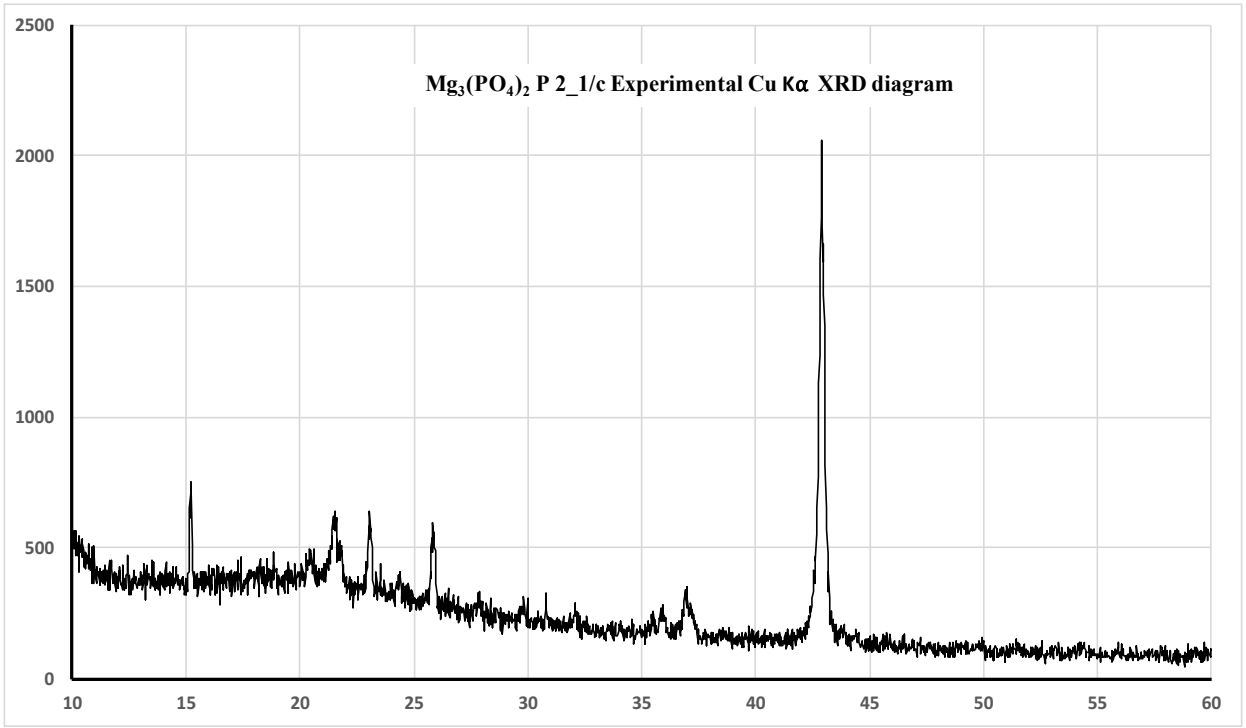

$Mg_3(PO_4)_2$ Main lines

Exp d (A°)	exp. I	Calc. d (A°)	Calc. I
5,82	20	5,58	10
4,37	5	4,36	22
4,14	12	4,12	23
4,10	8	4,08	25
3,86	17	3,84	83
3,45	17	3,44	100
2,43	10	2,42	25
2,11	100	2,13	22

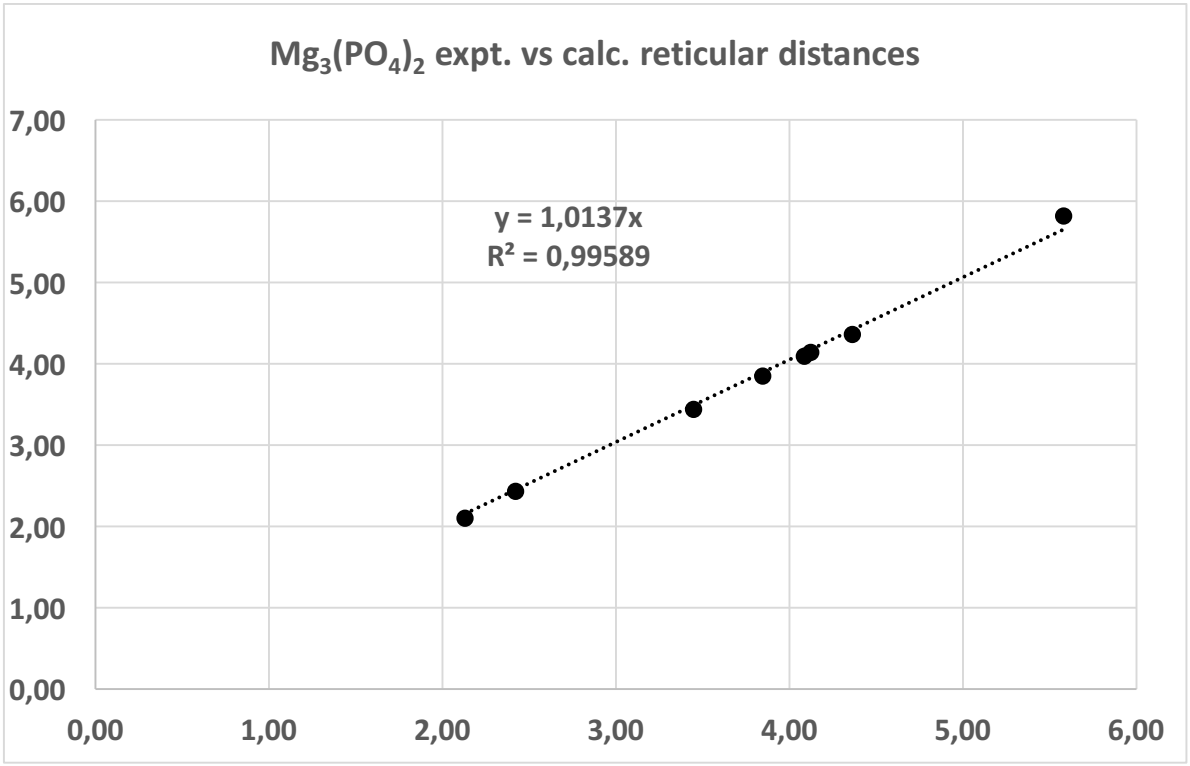

$AlPO_4$ P3221

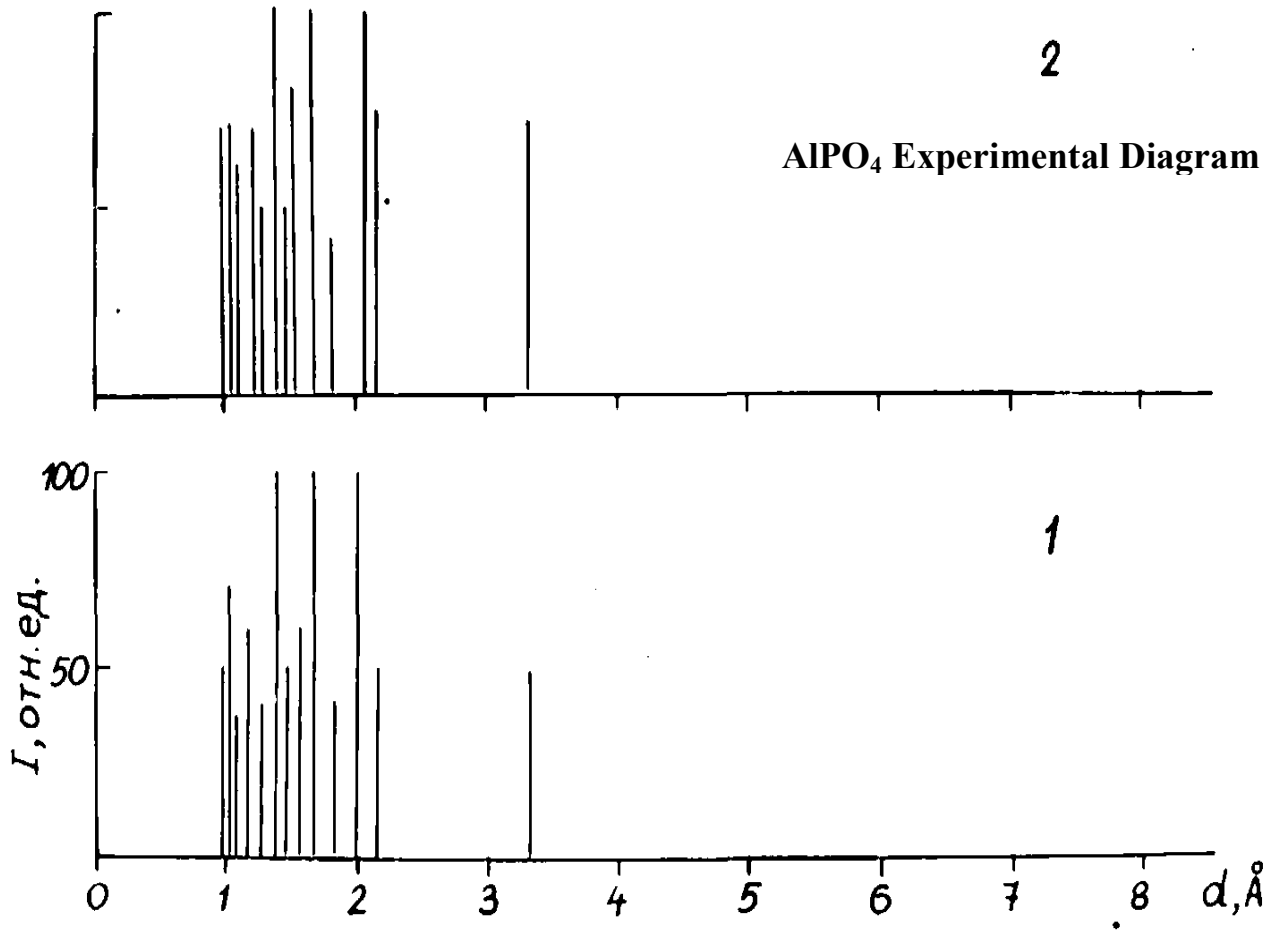

$AlPO_4$ Experimental Diagram

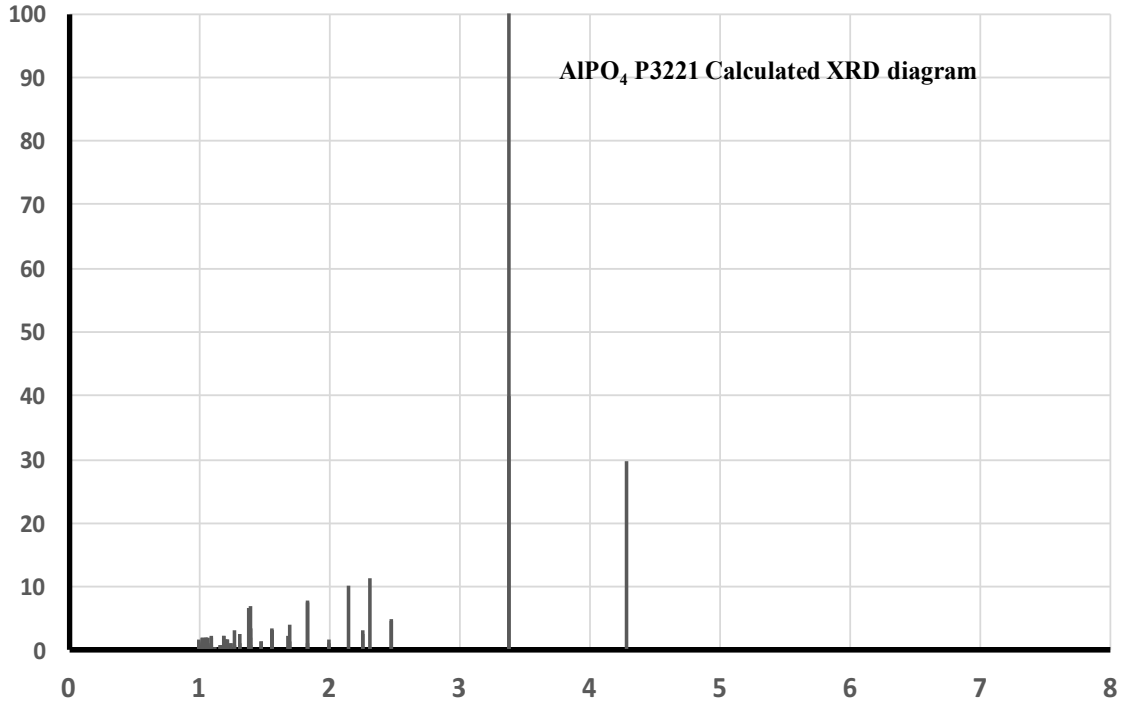

$AlPO_4$ P3221 Calculated XRD diagram

$AlPO_4$ Main lines

Exp d (A°)	exp. I	Calc. d (A°)	Calc. I
3,34	72	3,37	100
2,15	76	2,14	10
2,09	100	2,10	1,5
1,82	41	1,83	15
1,64	100	1,64	0,5
1,35	100	1,38	16

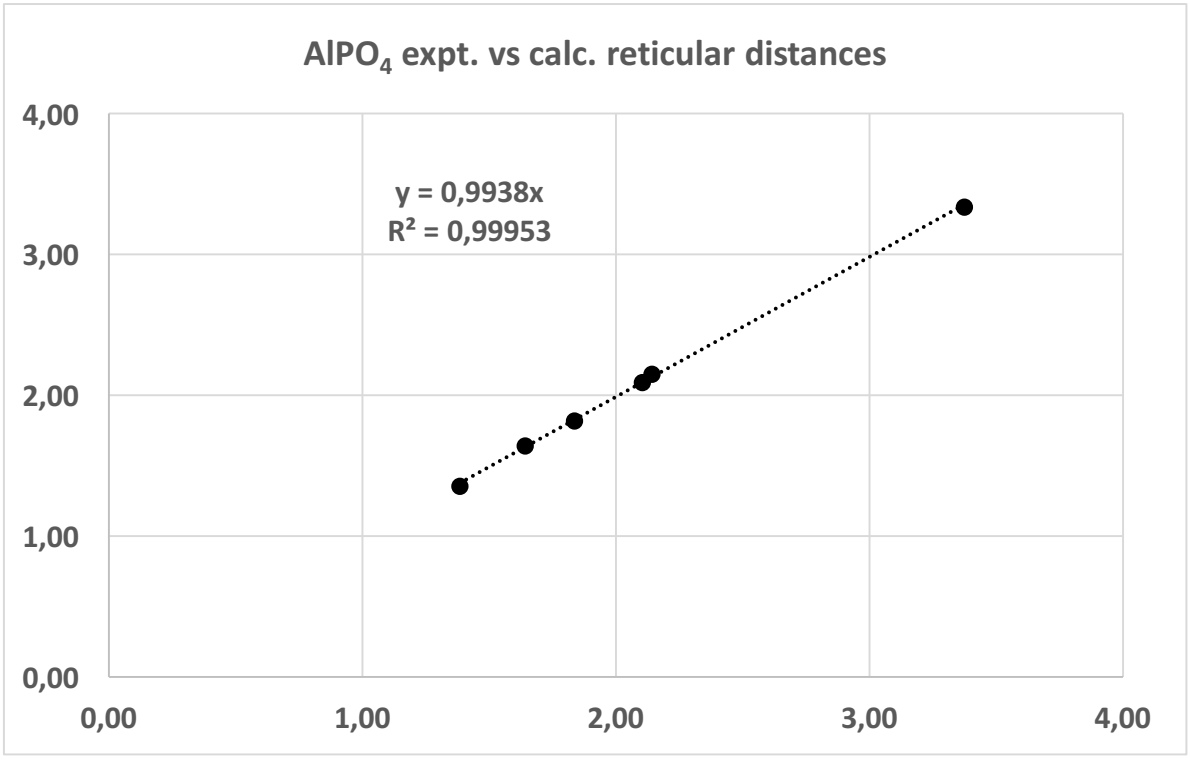

BPO_4 I-4

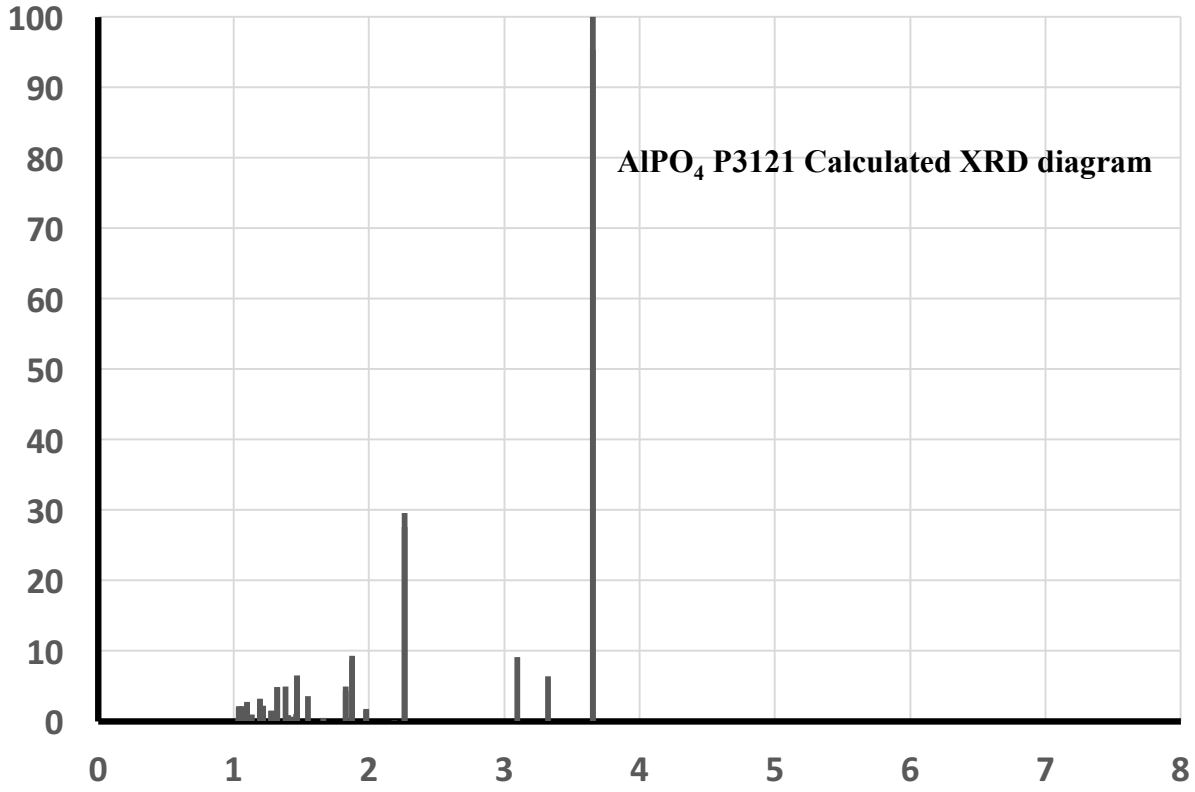
AlPO4 P3121 Calculated XRD diagram
100
90
80
70
60
50
40
30
20
10
0
0
1
2
3
4
5
6
7
8

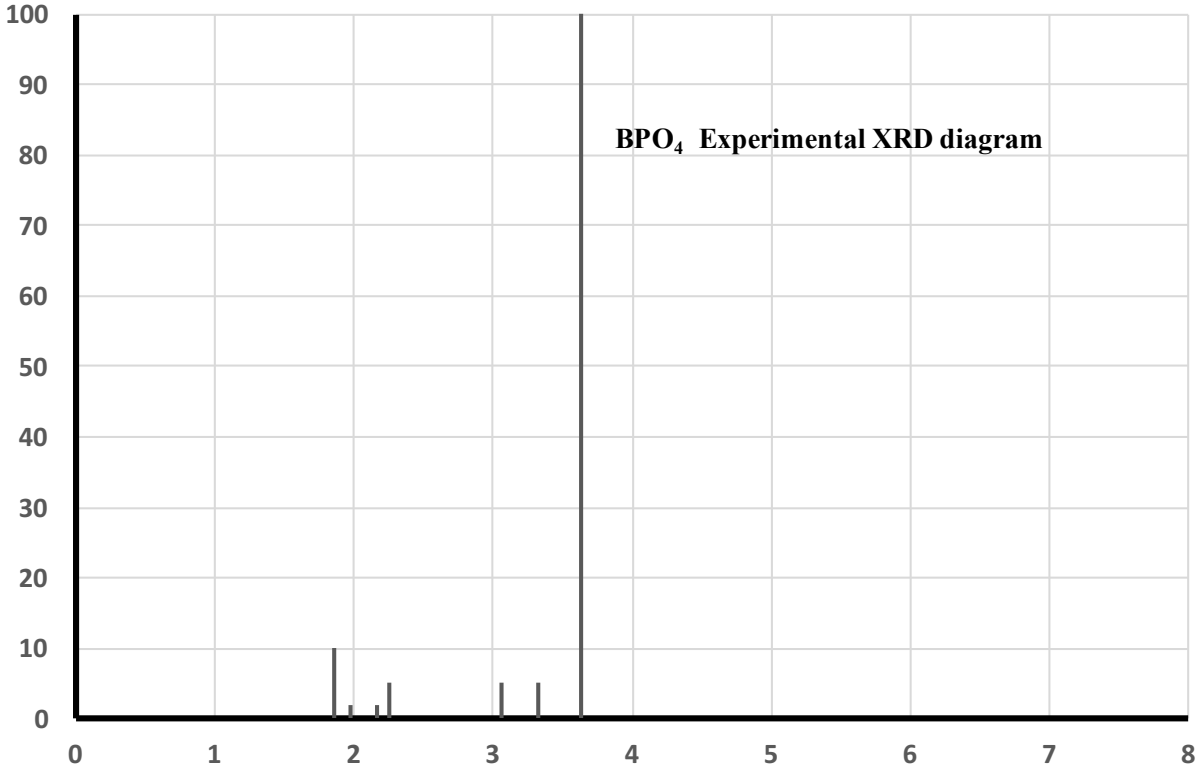
BPO4 Experimental XRD diagram
100
90
80
70
60
50
40
30
20
10
0
0
1
2
3
4
5
6
7
8

BPO_4 Main lines

Exp d (A°)	exp. I	Calc. d (A°)	Calc. I
3,63	100	3,65	100
3,32	5	3,33	6
3,06	5	3,09	10
2,25	5	2,26	30
2,17	2	2,19	1
1,97	2	1,98	3
1,86	10	1,88	10

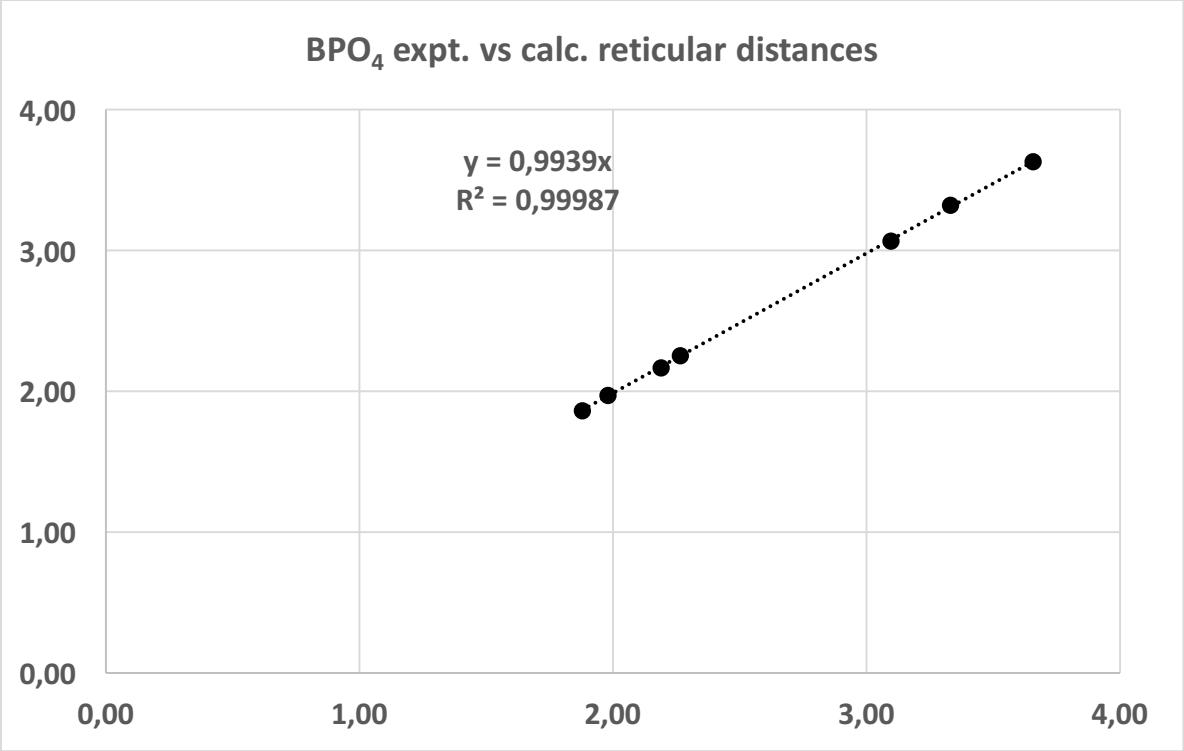

TiP_2O_7 Pa-3

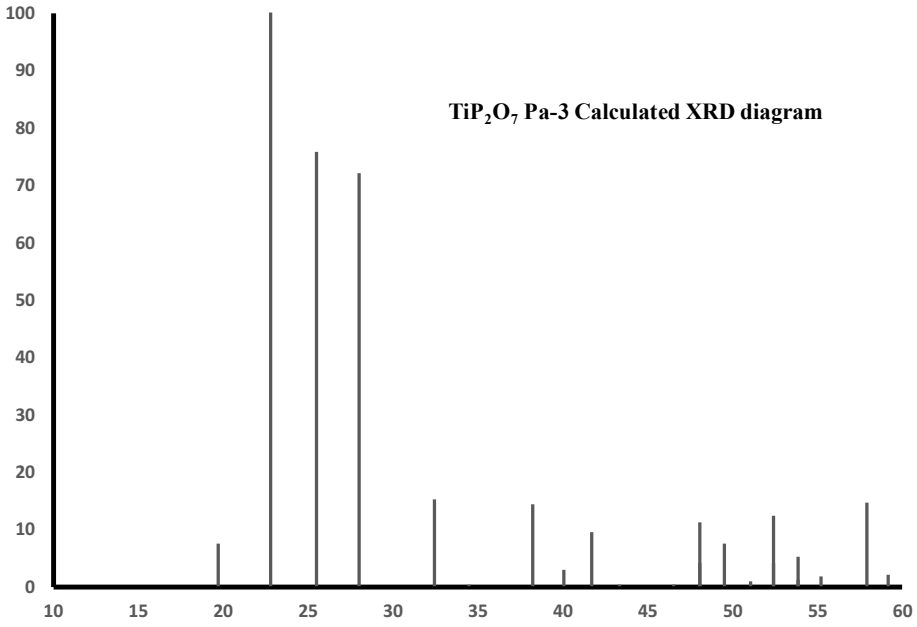

TiP_2O_7 Pa-3 Calculated XRD diagram

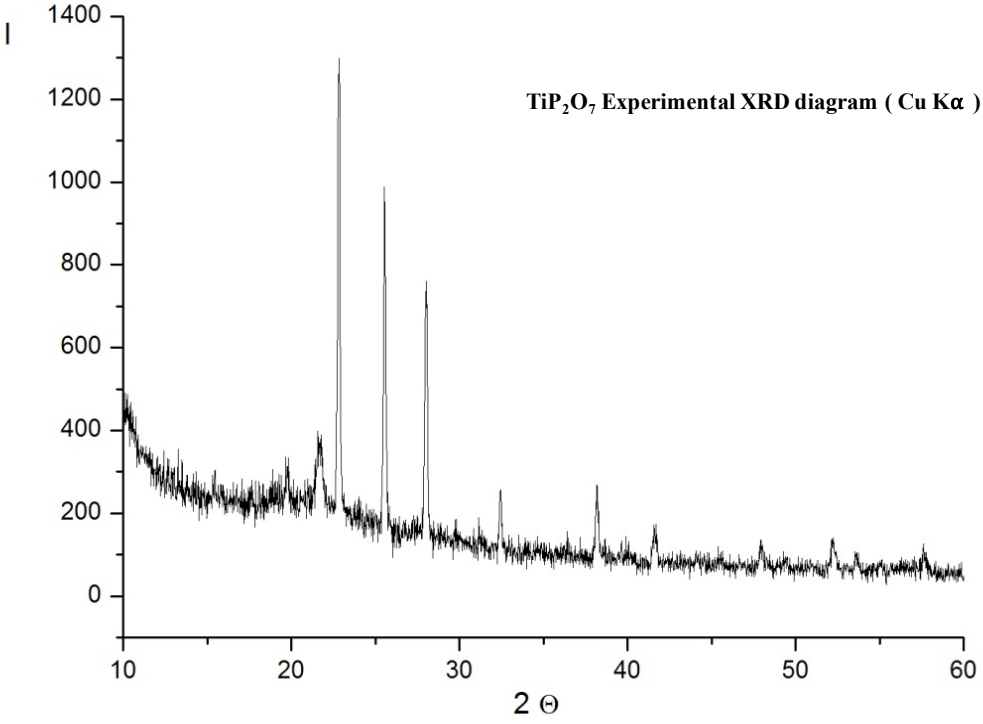

TiP_2O_7 Experimental XRD diagram (Cu Kα)

TiP_2O_7 Main lines

Exp d (A°)	exp. I	Calc. d (A°)	Calc. I
4,52	11	4,50	8
3,91	100	3,90	100
3,50	79	3,49	76
3,20	57	3,18	72
2,76	12	2,76	15
2,36	18	2,35	14
2,18	8	2,16	9
1,92	6	1,89	11
1,76	8	1,74	12

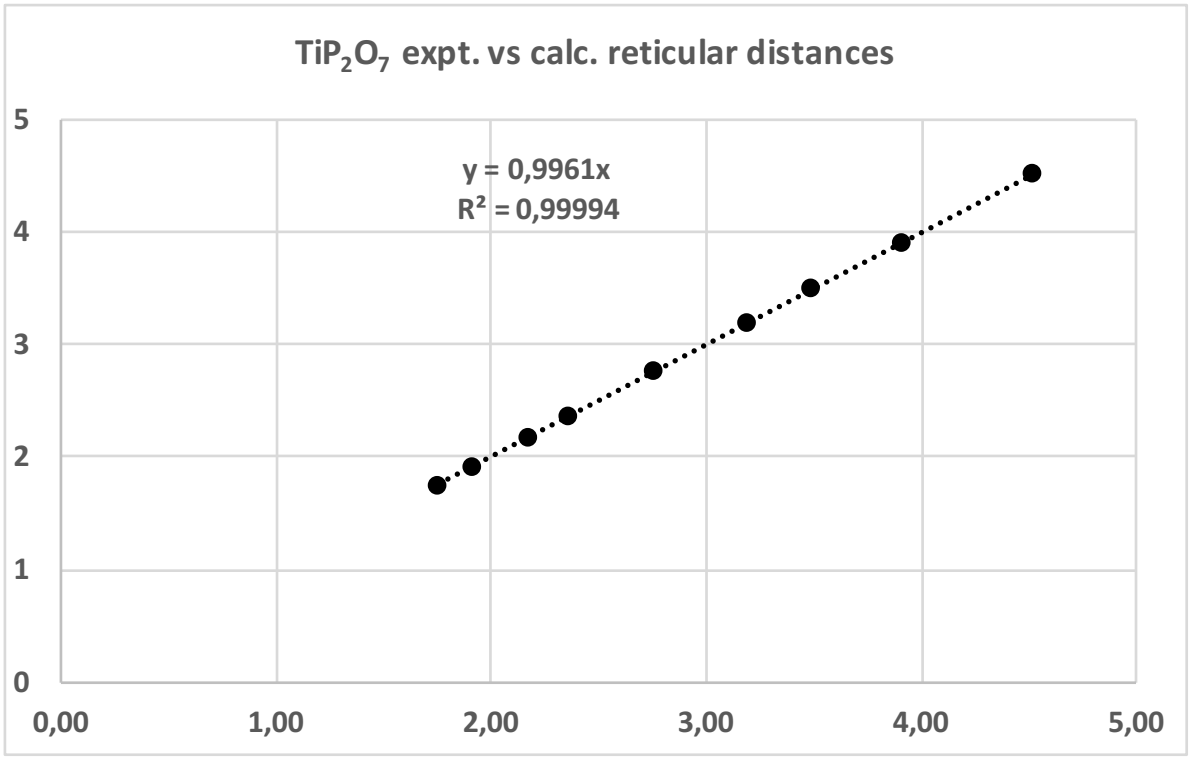

SiP_2O_7 Pa-3

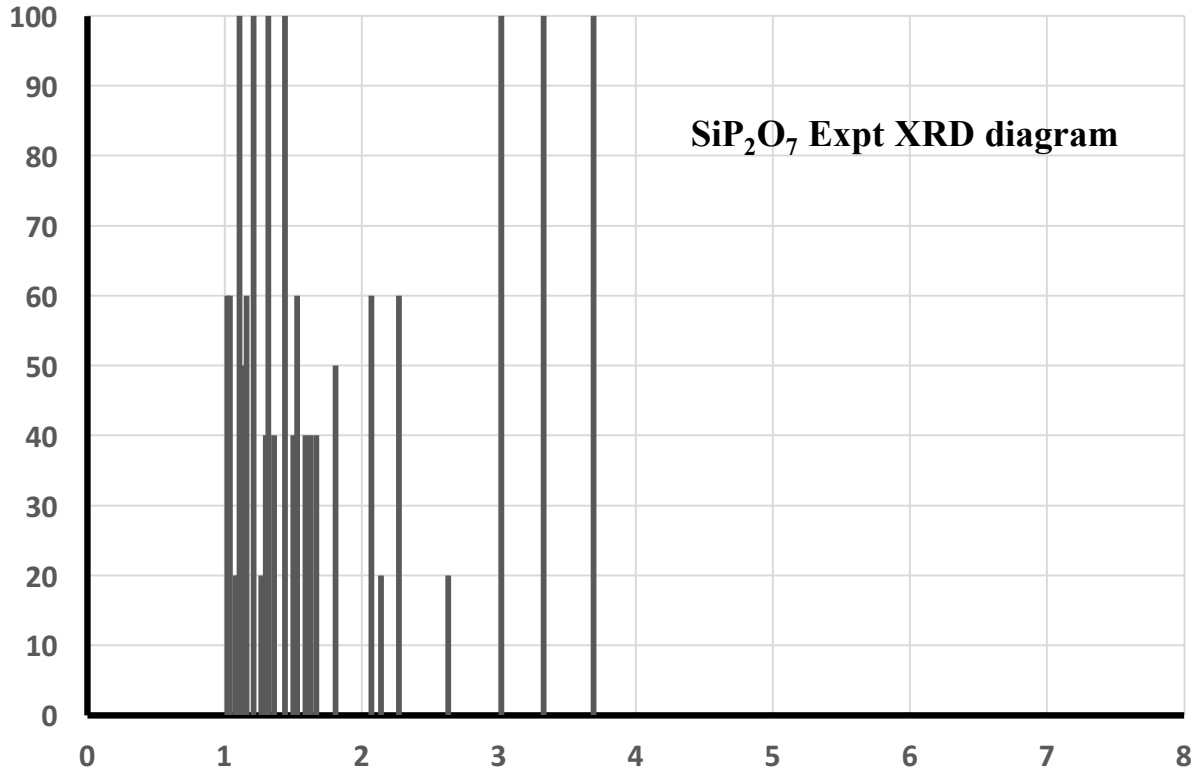
100
90
80
70
60
50
40
30
20
10
0
0
1
2
3
4
5
6
7
8
SiP_2O_7 Expt XRD diagram

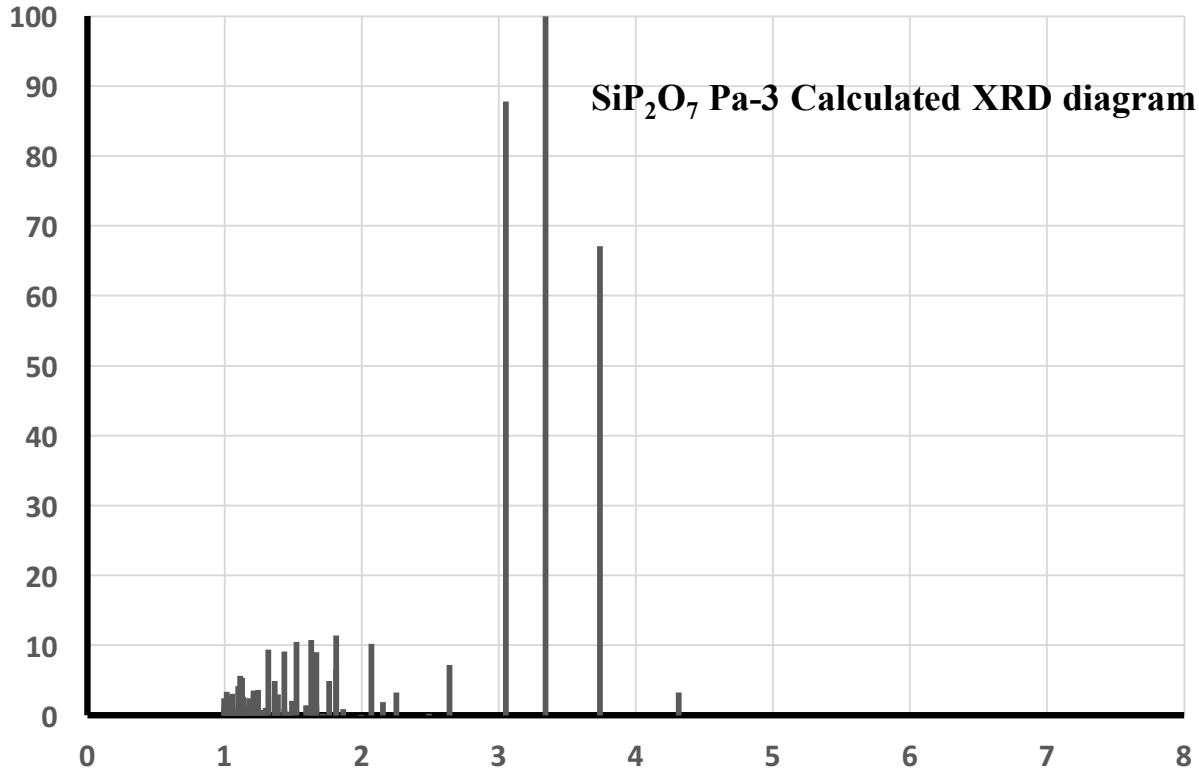
100
90
80
70
60
50
40
30
20
10
0
0
1
2
3
4
5
6
7
8
SiP_2O_7 Pa-3 Calculated XRD diagram

SiP_2O_7 Main lines

Exp d (A°)	exp. I	Calc. d (A°)	Calc. I
3,69	100	3,74	67
3,33	100	3,34	100
3,02	100	3,05	88
2,63	20	2,64	7
2,27	60	2,25	3
2,14	20	2,16	2
2,07	60	2,07	10
1,81	50	1,81	18
1,67	40	1,67	11

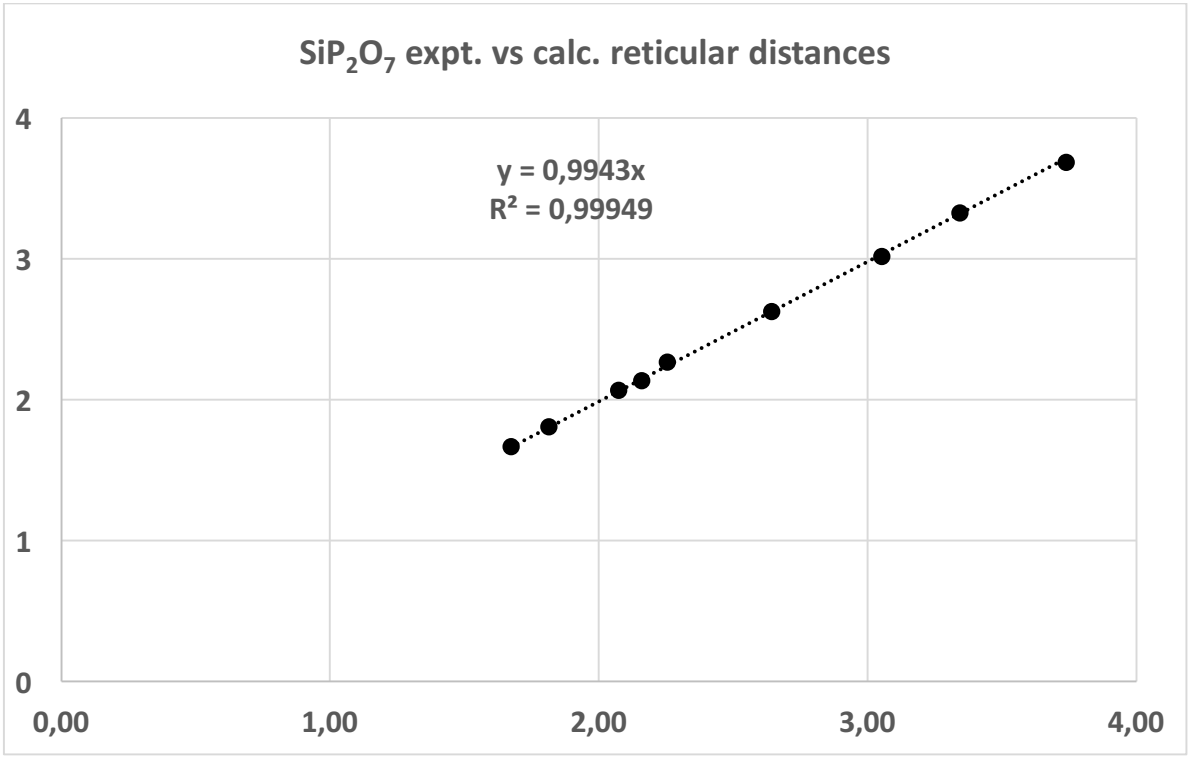

GeP_2O_7 Pa-3

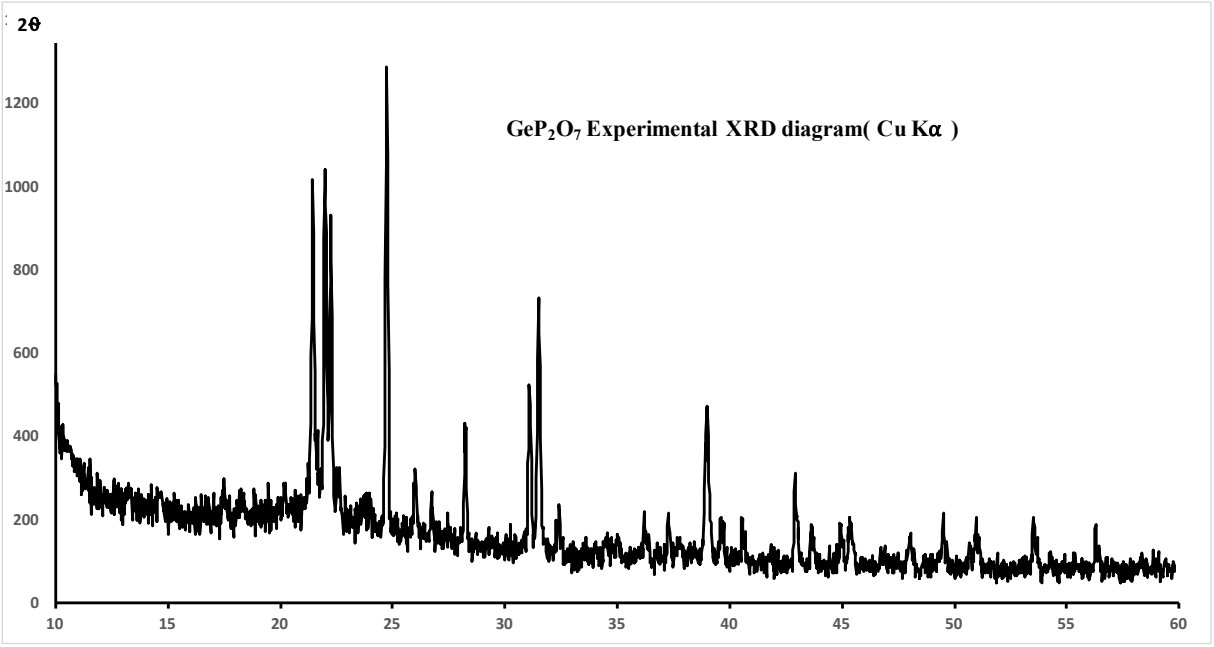
2θ
1200
1000
800
600
400
200
0
10
15
20
25
30
35
40
45
50
55
60
GeP2O7 Experimental XRD diagram(Cu Kα)

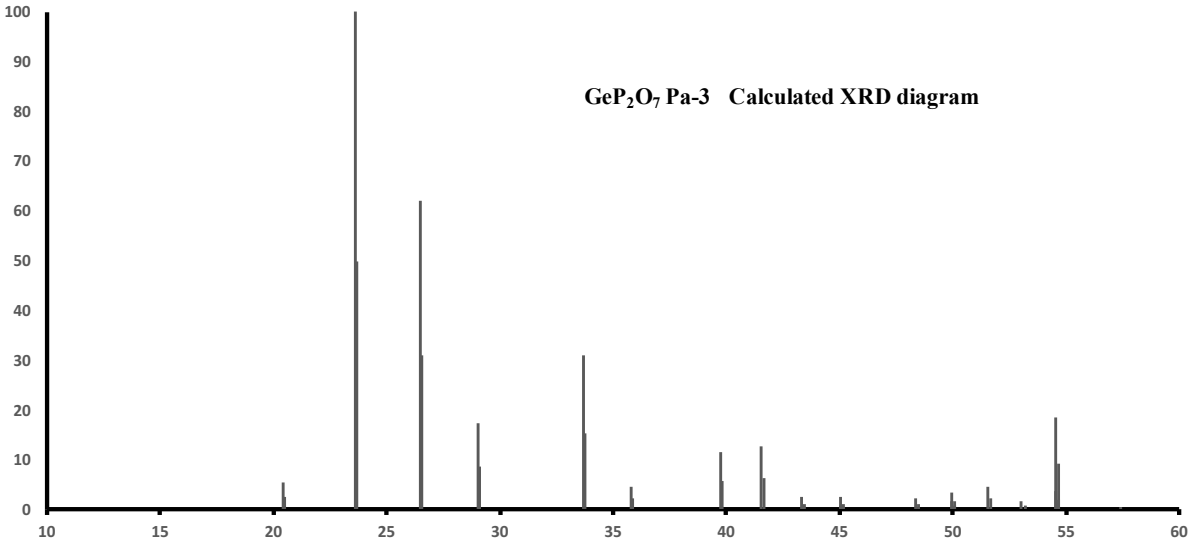
100
90
80
70
60
50
40
30
20
10
0
10
15
20
25
30
35
40
45
50
55
60
GeP2O7 Pa-3 Calculated XRD diagram

GeP_2O_7 Main lines

Exp d (A°)	exp. I	Calc. d (A°)	Calc. I
4,04	81	4,34	5
3,99	72	4,34	3
3,60	100	3,76	100
3,14	33	3,07	25
2,88	41	2,66	46
2,84	57	2,51	5
2,31	36	2,27	18
2,11	24	2,17	19
1,89	12	2,09	4
2,01	15	2,01	6
1,84	17	1,82	11
1,79	16	1,77	3
1,71	16	1,73	26
1,63	15	1,64	11

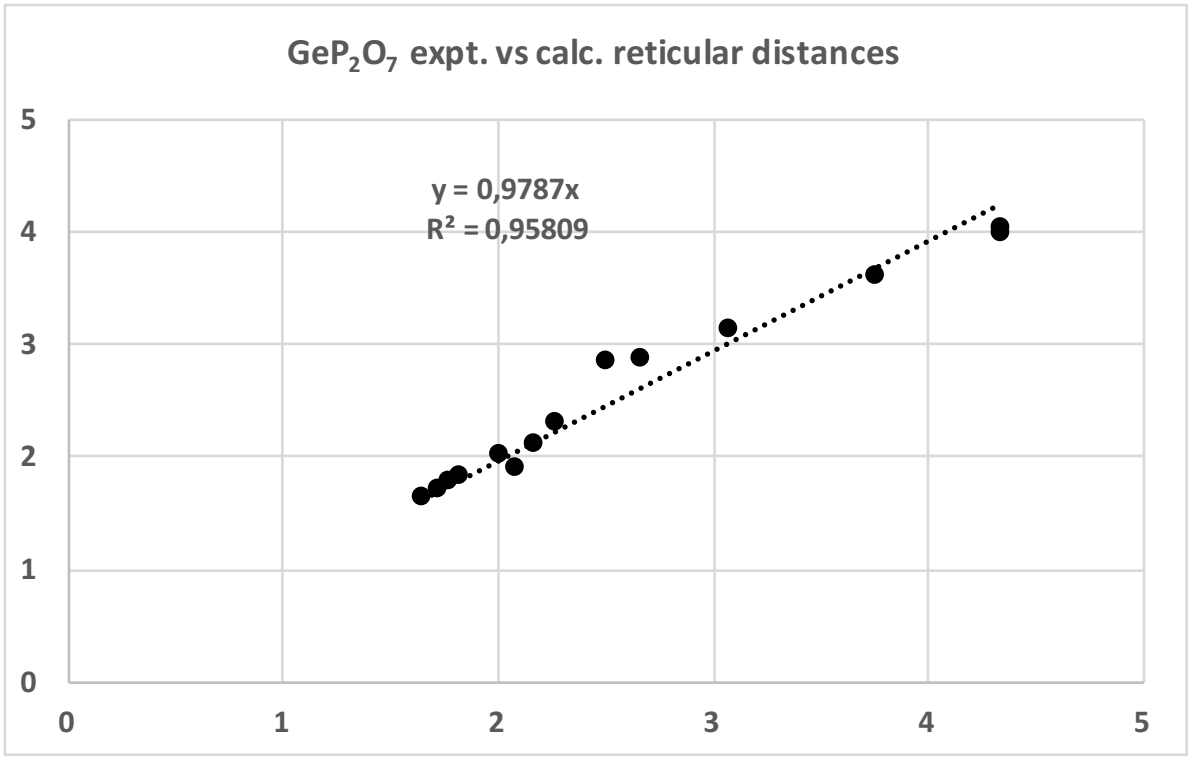

SnP_2O_7 Pa-3

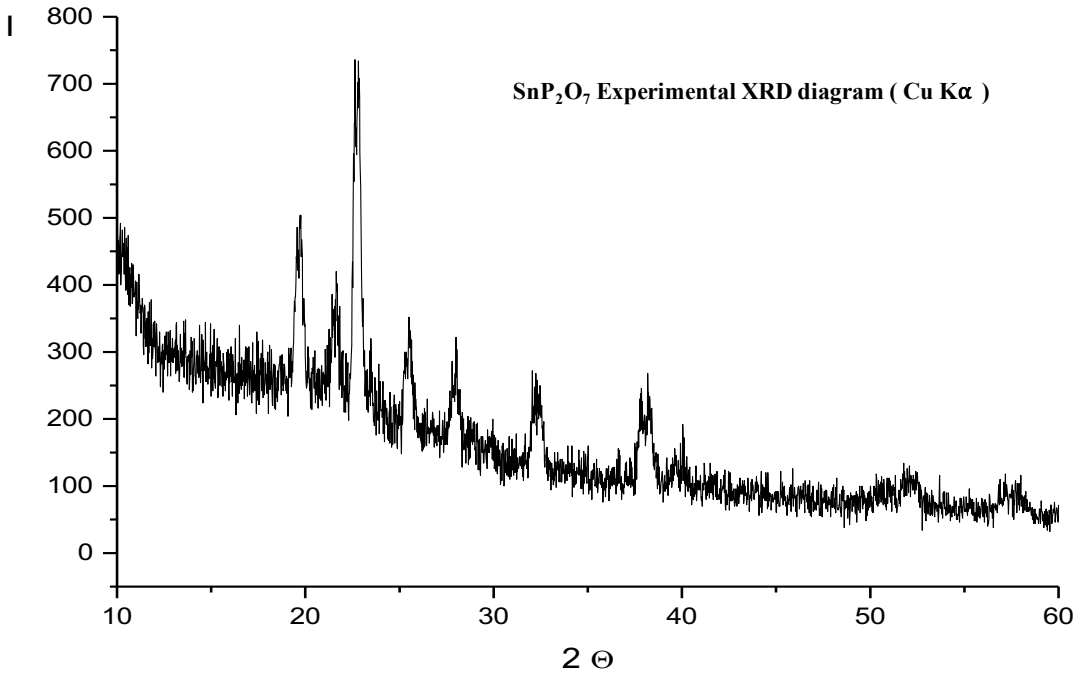
I
800
700
600
500
400
300
200
100
0
10
20
30
40
50
60
2 Θ
SnP2O7 Experimental XRD diagram (Cu Kα)

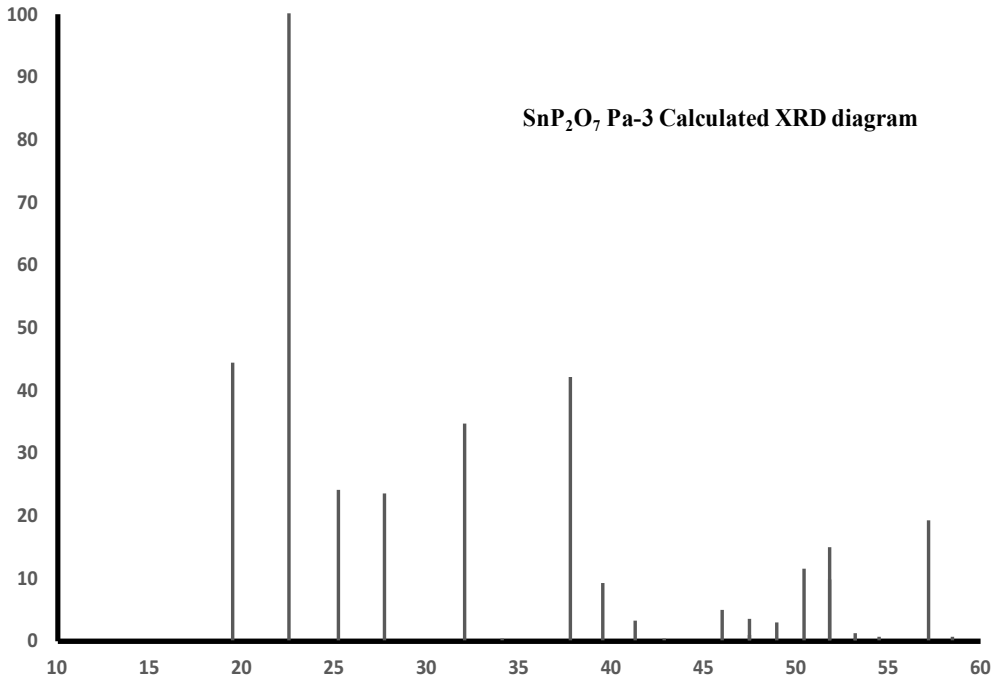
100
90
80
70
60
50
40
30
20
10
0
10
15
20
25
30
35
40
45
50
55
60
SnP2O7 Pa-3 Calculated XRD diagram

SnP_2O_7 Main lines

Exp d (A°)	exp. I	Calc. d (A°)	Calc. I
4,54	50	4,56	44
3,89	100	3,95	100
3,48	27	3,53	24
3,17	19	3,22	23
2,75	25	2,79	35
2,36	22	2,38	42
2,25	9	2,28	8
1,75	6	1,76	12

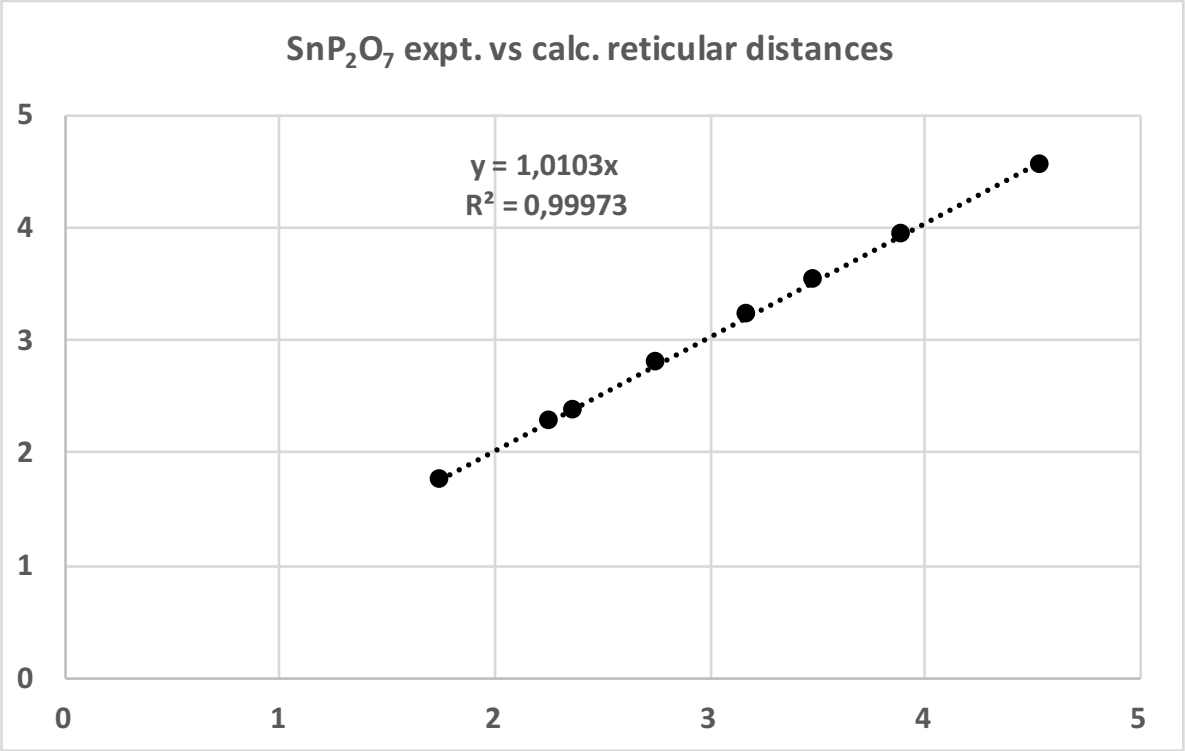

(1) K. Momma and F. Izumi, “VESTA 3 for three-dimensional visualization of crystal, volumetric and morphology data,” J. Appl. Crystallogr., 2011, 1272–1276.

BET Areas

The following table provides the BET surface areas measured on the considered phosphates after calcination at 973 K:

Solid	SG	BET area $m^2.g^{-1}$
$Mn_2P_2O_7$	C2/m	6
$CrPO_4$	Cmcm	65
$Co_3(PO_4)_2$	P-1	91
$Ni_3(PO_4)_2$	P1	29
$FePO_4$	P3121	17
$Mg_3(PO_4)_2$	P2_1/c	46
$AlPO_4$	P3221	15
BPO_4	I-4	12
TiP_2O_7	Pa-3	27
SiP_2O_7	Pa-3	35
GeP_2O_7	Pa-3	42
SnP_2O_7	Pa-3	76

IR Spectra of catalysts

In the following spectra, the absorbance is plotted as function of wavenumber. Spectrum 1 corresponds to the freshly prepared catalysts, and spectrum 2 to the same material after calcination at 1073K.

All catalyst present bands in the 3400-3800 cm^{-1} range of wavenumbers, specific of ν(OH) vibration, and revealing the occurrence of surface hydroxyls groups.

The bands in the vicinity of 3660 cm^{-1} have been assigned in ref [41] of main text to the OH stretching of free surface POH groups.

$Ni_3(PO_4)_2$

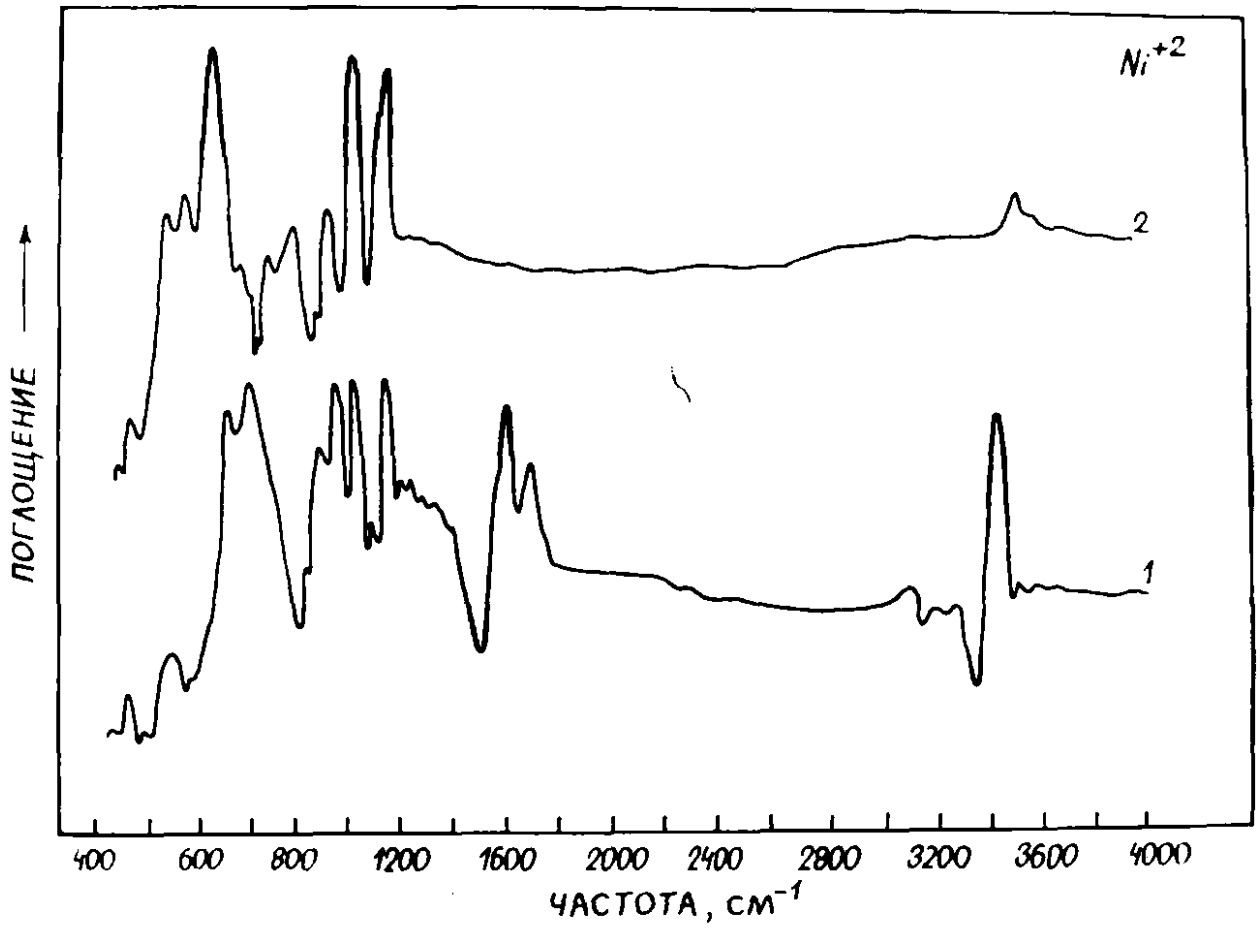

$Co_3(PO_4)_2$

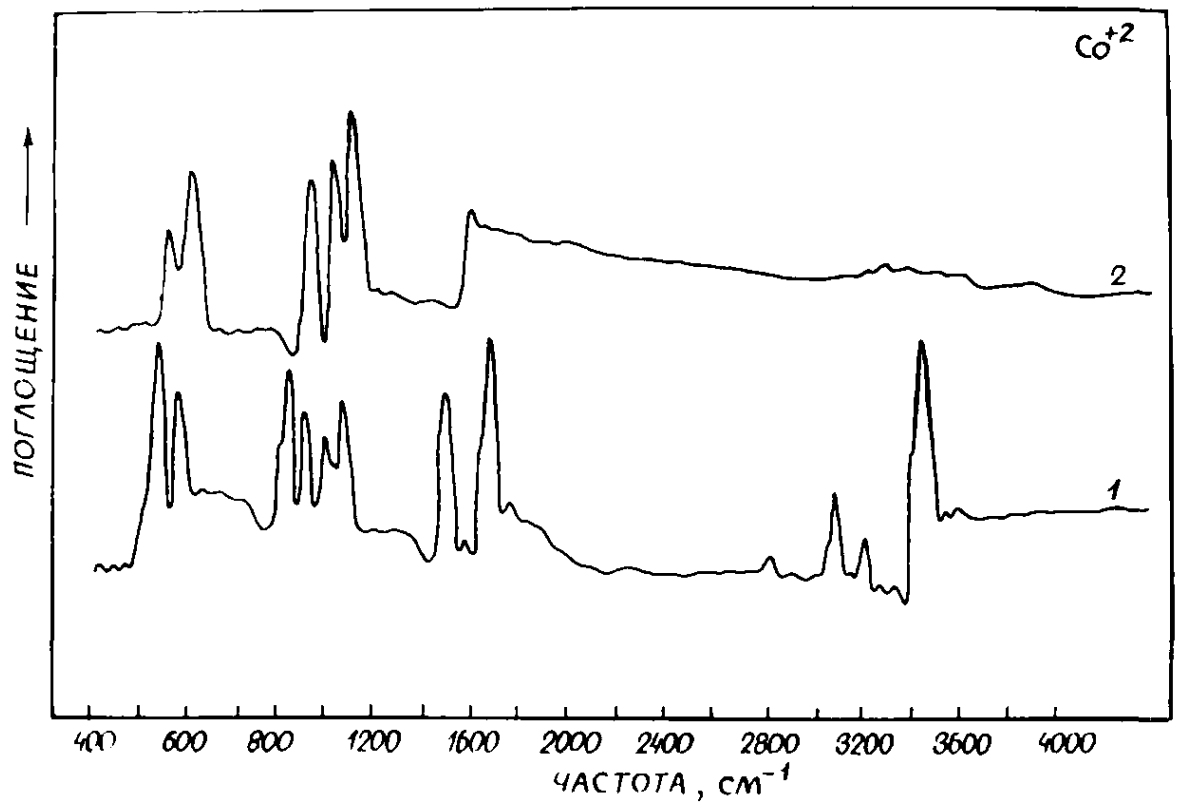
Co+2
2
1
ПОГЛОЩЕНИЕ
400
600
800
1200
1600
2000
2400
2800
3200
3600
4000
ЧАСТОТА, см-1

$CrPO_4$

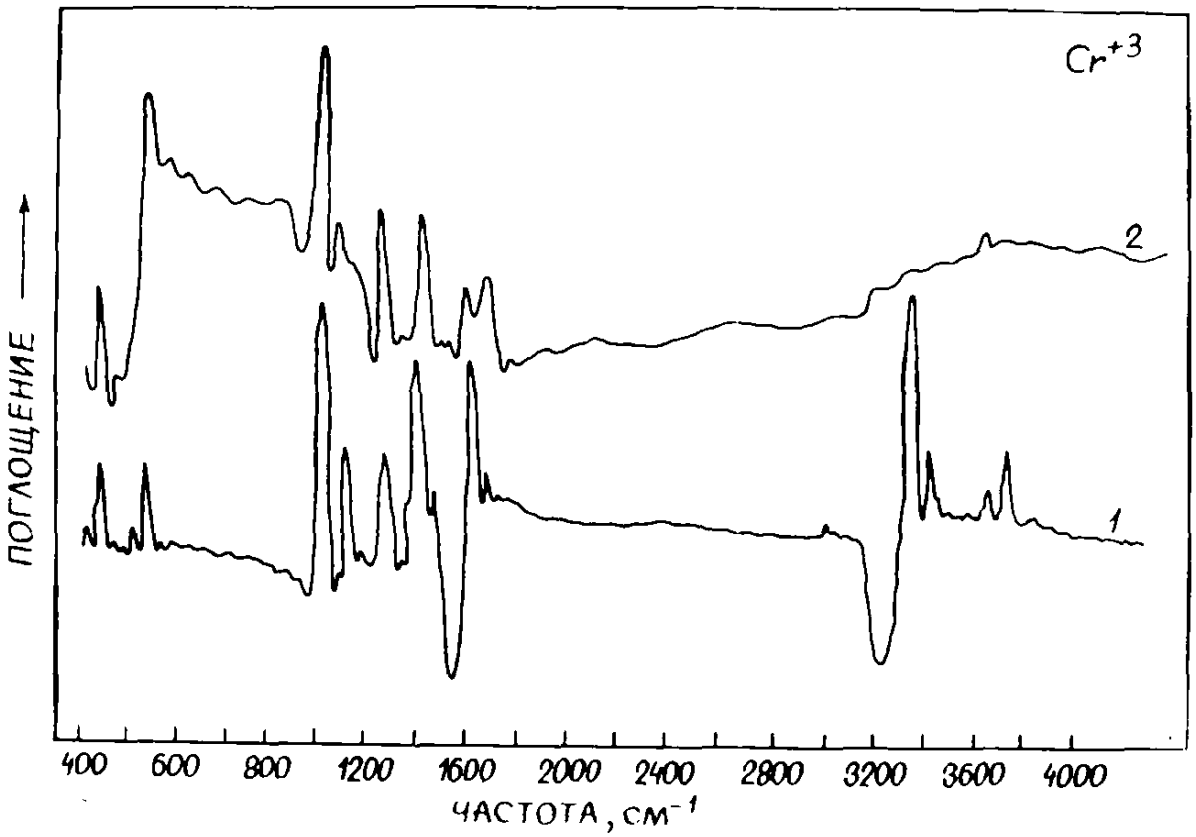
Cr+3
2
1
ПОГЛОЩЕНИЕ
400
600
800
1200
1600
2000
2400
2800
3200
3600
4000
ЧАСТОТА, см⁻¹

$FePO_4$

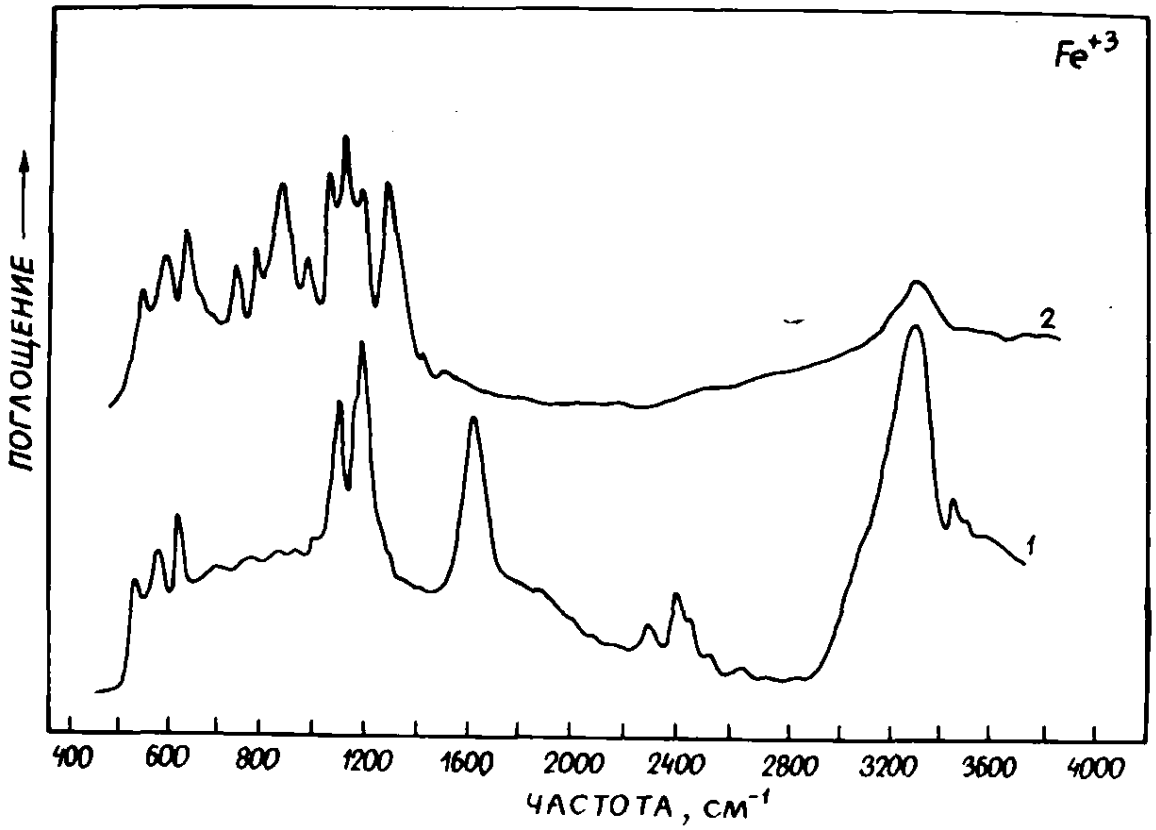
Fe+3
ПОГЛОЩЕНИЕ
2
1
400
600
800
1200
1600
2000
2400
2800
3200
3600
4000
ЧАСТОТА, см-1

$AlPO_4$

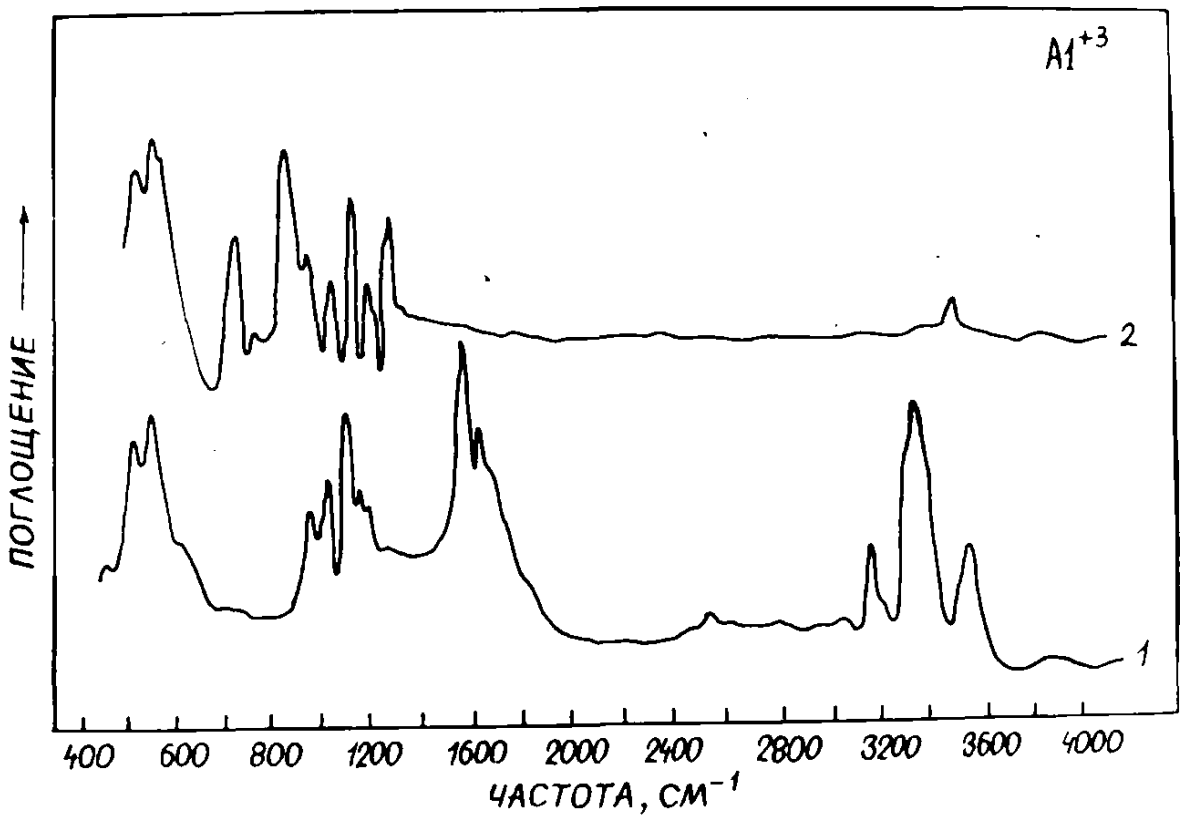
Al+3
ПОГЛОЩЕНИЕ
2
1
400
600
800
1200
1600
2000
2400
2800
3200
3600
4000
ЧАСТОТА, СМ⁻¹

BPO_4

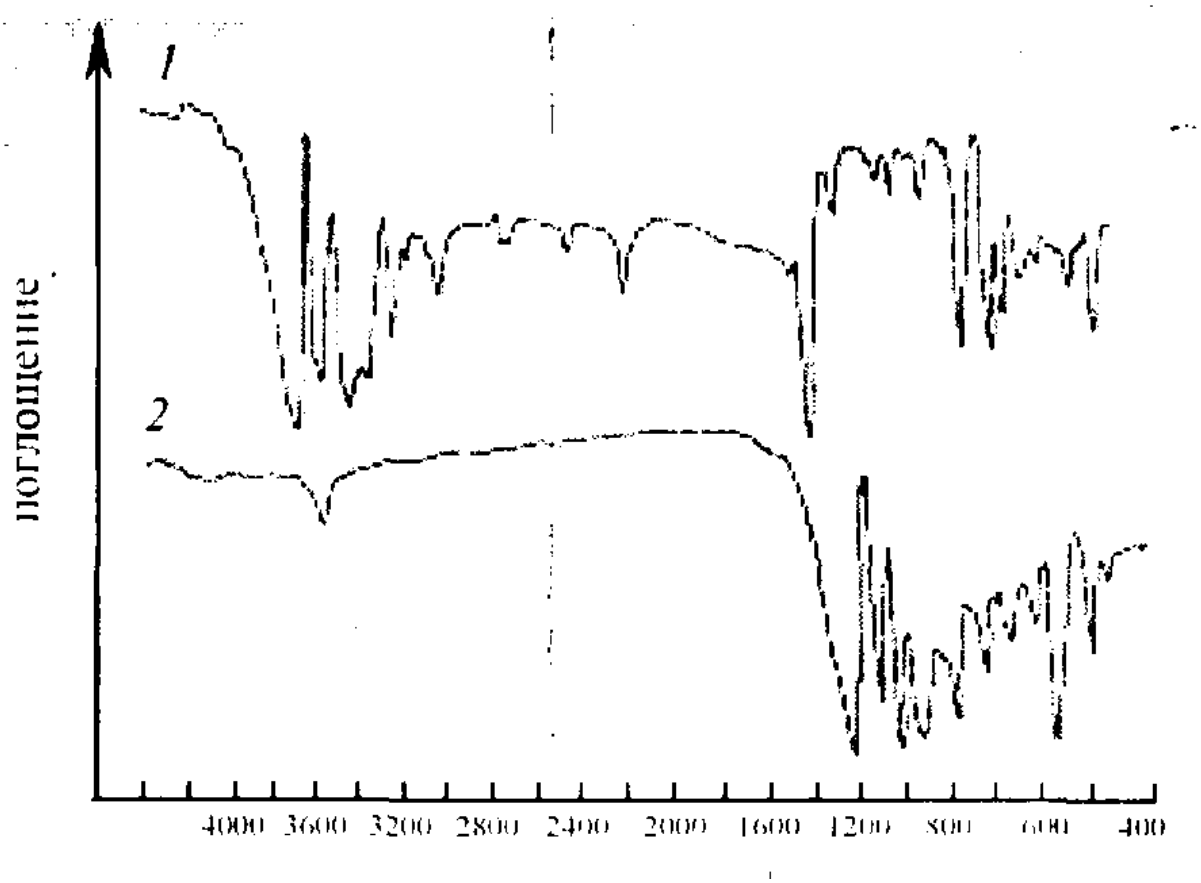
1
2
поглощение
4000
3600
3200
2800
2400
2000
1600
1200
800
600
400

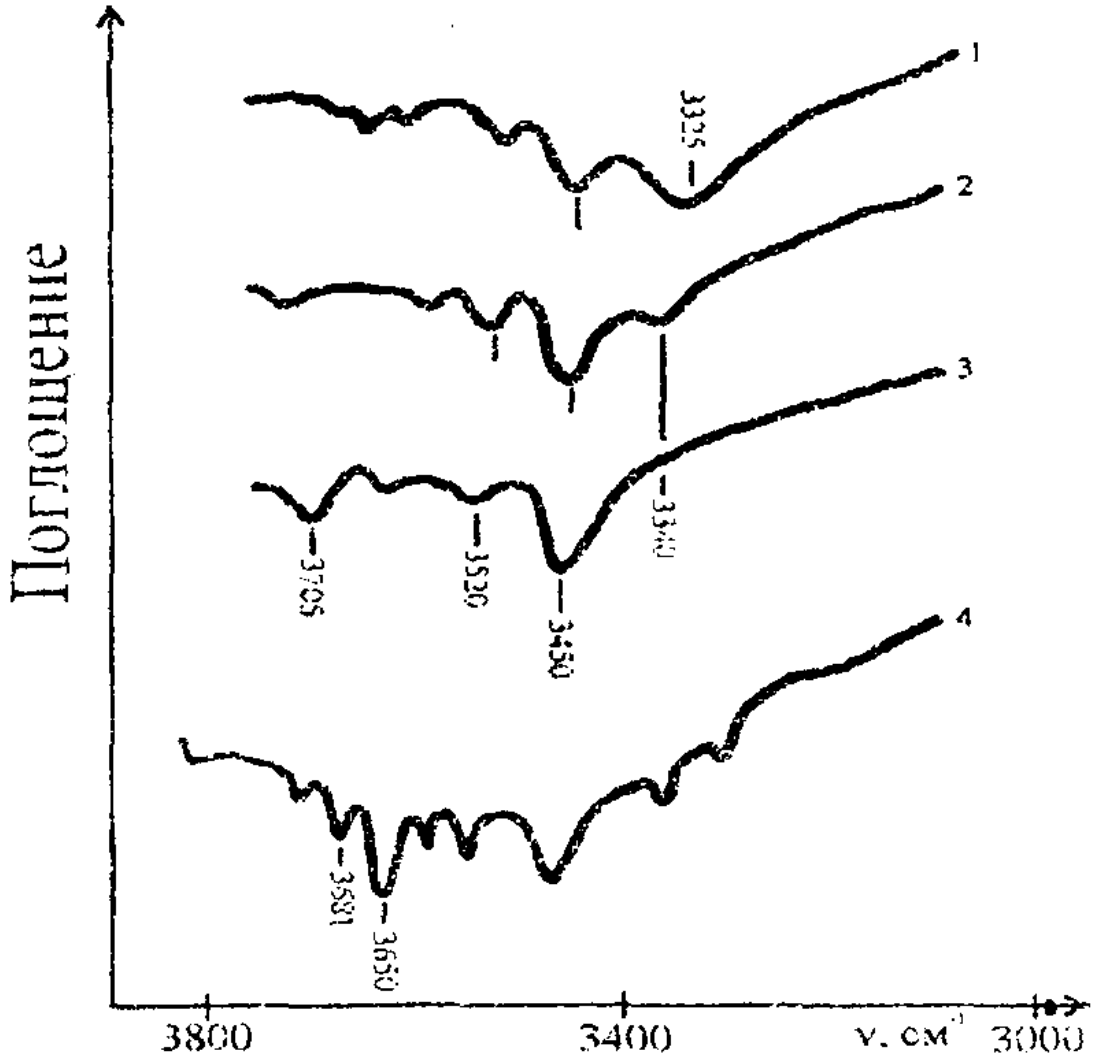

Infrared spectra of BPO_4 sample in the domain of surface OH vibrations : 1- processed in vacuo 4 hours at 900 *K*; 2 - after ammonia adsorption at 300 *K*; 3 – Evacuated at 423 *K*, 30 minutes; 4 - Evacuated at 673 *K*, 30 minutes.

SI-2 – Bench-scale catalyst testing equipment

All catalyst were compared in a specially designed flow circulation reactor with reaction mixture quenching (2) as schematically presented below:

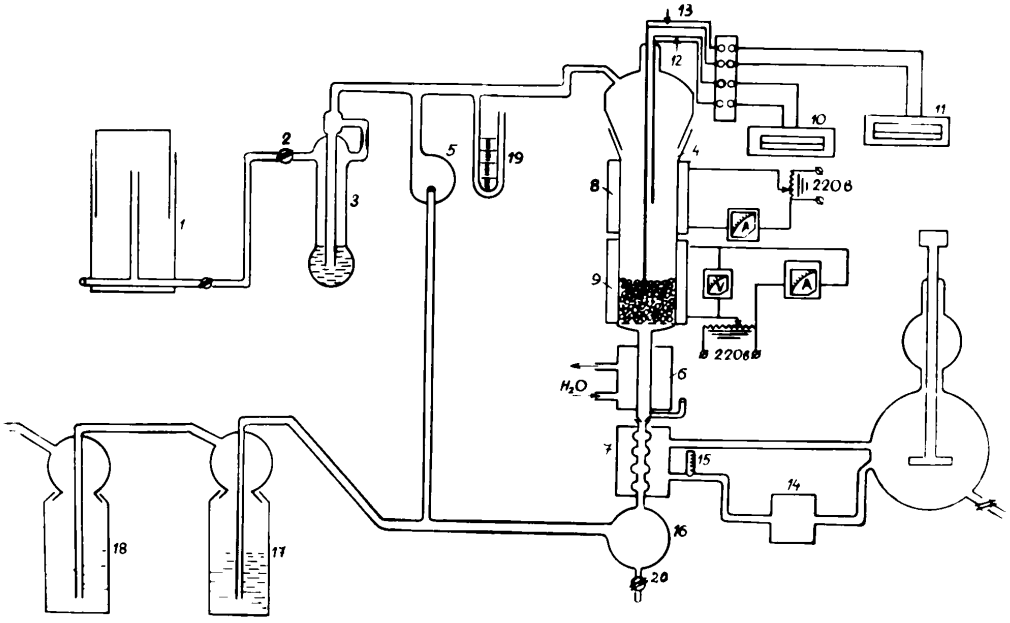

1: Reaction mixture tank (methane+oxygen)

5: Recycle pump

9: Catalyst pellets inside the reactor

6: First stage cooler (room temperature tap water)

7: Second stage cooler for condensation of formaldehyde and water produced by the reaction (circulating fluid, water at 5-10 °C).

15, 16 : Condensate collector (aqueous formaldehyde solution)

17, 18 : Condensate scrubbers

The feed rate of reaction mixture is set between 3 and15 $Nl.hr^{-1}$, while the recycle flow-rate is maintained at 150 $Nl.hr^{-1}$ so as to ensure the condition of equivalence with a perfectly stirred differential reactor.

(2) Gomonai, V.I., *Doctoral (Chem.) Dissertation*, Uzhgorod State Univ., 1990.

SI-3 Supplementary Tables

Table SI-3-1: Bader charges in electronic units for DFT optimized reference structures of phosphate bulk catalysts. Q_M : averaged Bader charge on M atoms; Q_{MF} : formal charge of M ion; Q_P : averaged Bader charge on P atoms; Q_{Oa} : averaged Bader charge on Oa atoms; averaged Q_{Ob}Bader charge on Ob atoms. Formal charges for P and O are +5 and -2 respectively.

Solid	Q_M	Q_{MF}	Q_P	Q_{Oa}	Q_{Ob}
$Mn_2P_2O_7$	1.533	2	3.687	-1.478	-1.568
$CrPO_4$	1.815	3	3.652	-1.368	
$Co_3(PO_4)_22_2$	1.312	2	3.656	-1.402	
$Ni_3(PO_4)_2$	1.236	2	3.616	-1.368	
$FePO_4$	1.703	3	3.703	-1.351	
$Mg_3(PO_4)_2$	1.697	2	3.694	-1.558	
$AlPO_4$	2.492	3	3.756	-1.562	
BPO_4	2.380	3	3.756	-1.534	
TiP_2O_7	2.380	4	3.751	-1.391	-1.538
SiP_2O_7	3.262	4	3.772	-1.543	-1.548
GeP_2O_7	2.640	4	3.776	-1.438	-1.564
SnP_2O_7	2.692	4	3.756	-1.441	-1.556

Table SI-3-2: Experimental specific total acidities H^0 in μmol.m^{-2}, catalytic oxidation rates *w* in 10^9 mol.m^{-2}.s^{-1} and selectivities in moles % of oxidation products for phosphate catalysts at 873 K, atmospheric pressure and molar ratio O_2/CH_4 = 0.5. Acidities and selectivities in formaldehyde are correlated.

Solid	H^0	w	$\%CH_2O$	%CO	$\%CO_2$
$Mn_2P_2O_7$	0.09	185	1	15	84
$CrPO_4$	0.35	76.3	3	19	78
$Co_3(PO_4)_2$	0.83	35.6	6	23	71
$Ni_3(PO_4)_2$	1.30	25.4	10	26	64
$FePO_4$	2.10	16.4	15	33	52
$Mg_3(PO_4)_2$	3.30	11.8	24	36	40
$AlPO_4$	5.00	8.76	38	35	27
BPO_4	6.90	6.28	51	32	17
TiP_2O_7	10.6	4.85	79	22	9
SiP_2O_7	13.6	3.55	83	12	5
GeP_2O_7	15.2	2.94	86	11	3
SnP_2O_7	16.5	2.45	96	3	1

Table SI-3-3: Comparison of experimental and simulated catalytic oxidation rates *w* in 10^9 mol.m^{-2}.s^{-1} and selectivities in moles % of oxidation products for phosphate catalysts at 873 K, atmospheric pressure and molar ratio $O_2/CH_4 = 0.5$.

Solid	w_{exp}	w_{sim}	$\%CH_2O$	$\%CH_2Osim$
$Mn_2P_2O_7$	185	185.0	1	4.1
$CrPO_4$	76.3	94.4	3	4.8
$Co_3(PO_4)_2$	35.6	61.8	6	7.4
$Ni_3(PO_4)_2$	25.4	25.3	10	11.3
$FePO_4$	16.4	25.6	15	13.8
$Mg_3(PO_4)_2$	11.8	11.6	24	23.7
$AlPO_4$	8.76	8.41	38	37.1
BPO_4	6.28	6.18	51	56.6
TiP_2O_7	4.85	8.99	79	77.5
SiP_2O_7	3.55	14.6	83	86.8
GeP_2O_7	2.94	53,4	86	87.7
SnP_2O_7	2.45	62,4	96	90.7

Solid	%CO	%COsim	$\%CO_2$	$\%CO_2sim$
$Mn_2P_2O_7$	15	16.8	84	79.1
$CrPO_4$	19	21.5	78	71.4
$Co_3(PO_4)_2$	23	21.1	71	71.5
$Ni_3(PO_4)_2$	26	23.7	64	65.0
$FePO_4$	33	33.9	52	52.3
$Mg_3(PO_4)_2$	36	36.5	40	39.8
$AlPO_4$	35	34.9	27	28.0
BPO_4	32	27.3	17	16.1
TiP_2O_7	22	11.4	9	11.1
SiP_2O_7	12	5.9	5	7.7
GeP_2O_7	11	3.2	3	9.1
SnP_2O_7	3	2.3	1	7,0

SI-4 Kinetic Model

As presented in the main text, we assume that methane oxidation can be decomposed in the following elementary steps for each phosphate catalyst:

Step №	Reaction equation
1	O_2 (g) + 2Z ⇔ 2ZO
2	CH_4 (g) + ZO ⇔ $ZOHCH_3$
3	$ZOHCH_3$ + ZO ⇔ $ZOHCH_2$+ ZOH
4	$ZOHCH_2$ + ZO ⇔ $ZOHCH_2O$ + Z
5	$ZOHCH_2O$ ⇔ CH_2O (g) + ZOH
6	$ZOHCH_2O$+ ZO ⇔ ZHCOOH + ZOH
7	ZHCOOH ⇔ CO (g) + H_2O (g) + Z
8	ZHCOOH + ZO ⇔ CO_2 (g) + H_2O (g) + 2Z
9	2ZOH ⇔ H_2O (g) + ZO + Z

In these equations, Z represents a Lewis acidic cationic sites, with Z= P or Z=M. ZO is a Z surface site covered by an oxygen adatom.

$ZOHCH_3$ represents the surface species formed by the carbidic insertion of gaseous methane into a surface ZO bond, following a radicalar activation, forward step 2. See figure SI-5-1 in next section for a molecular model of this intermediate.

$ZOCH_2$ is produced in forward step 3 by oxidative dehydrogenation of $ZOHCH_3$, transferring one H atom to a vicinal ZO. See figure SI-5-2 in next section for a molecular model of this intermediate.

$ZOHCH_2O$ is produced in forward step 4 by oxidative transfer of an O atom from a vicinal ZO to $ZOCH_2$. See figure SI-5-3 in next section for a molecular model of this intermediate, which can also be described as a chemisorbed formaldehyde on a Z-OH surface group. This species will either desorb (forward step 5), or be oxidized by a vicinal ZO into a chemisorbed

formic acid species ZHCOOH (forward step 6). See figure SI-5-4 in next section for a molecular model of this last intermediate.

ZHCOOH either decomposes into CO and H_2O which desorb to gas phase (forward step 7) leaving a free Z site, or is further oxidized by a vicinal ZO into CO_2 and H_2O which desorb to gas phase (forward step 8).

Step 9 represents the associative desorption of water from two vicinal ZOH sites.

In what follows, we will distinguish steps 1, 2 and 9 involving reversible exchanges with the gas phase from steps 3, 4, 6, which describe the successive oxidation steps of a chemisorbed methane molecule at the surface, and from steps 5, 7 and 8 the desorption to gas phase of the final products formaldehyde, CO, CO_2 and H_2O. Since the experiments involve a differential reactor with continuous removal of products from the gas phase recycled at high flow-rate at fixed composition, we will consider steps 3, 4, 6, 5, 7 and 8 as very far from equilibrium, i.e. neglect rates of the reverse reactions.

Steps 1, 2 and 9 contribute to determine surface coverages by O, OH and CH_4 (and its products of oxidation in adsorbed state) as ZO, ZOH and ZOHCH3 sites competing for free Z sites according to a Langmuir-Hinshelwood scheme. The chemisorption of CH_4 on ZO can be considered as well as following the Eley-Rideal mechanism, however it also possible to consider it formally as the chemisorption on a Z site of methanol produced from CH_4 in the gas phase.

With [Z°] the total concentration of surface sites, the balance of surface sites in equilibrium with the gas phase may be written:

$$[Z^0] = [Z] + [ZO] + [ZOHCH3] + [ZOH] \qquad \text{eq. SI-4\_1}$$

Denoting by K_i the equilibrium constant for step i, [ZX] the concentrations of surface intermediates ZX, and P_y the partial pressures of gaseous species y, one gets:

$$\left(\frac{[ZO]}{[Z]}\right)^2 = P_{O_2}K_1 \qquad \text{eq. SI-4\_2}$$

$$\frac{[ZOHCH3]}{[ZO]} = P_{CH_4}K_2 \qquad \text{eq. SI-4\_3}$$

$$\frac{[ZOH]^2}{[Z][ZO]} = \frac{P_{H_2O}}{K_9} \qquad \text{eq. SI-4\_4}$$

Substituting eqs SI-4_2 to SI-4_4 into eq. SI-4_1, and dividing by [Z°]:

$$1 = \left(\frac{[Z]}{[Z^0]} + \frac{[Z]}{[Z^0]}\left(P_{O_2}K_1\right)^{1/2} + \frac{[ZO]}{[Z^0]}P_{CH_4}K_2 + \left(\frac{[ZO]}{[Z^0]}\frac{[Z]}{[Z^0]}\frac{P_{H_2O}}{K_9}\right)^{1/2}\right) \qquad \text{eq. SI-4\_5}$$

Eliminating further [ZO]:

$$1 = \frac{[Z]}{[Z^0]}\left(1 + \left(P_{O_2}K_1\right)^{1/2}\left(1 + P_{CH_4}K_2 + \left(P_{O_2}K_1\frac{P_{H_2O}}{K_9}\right)^{1/2}\right)\right)$$

Assuming $K_1 \sim K_9$ and since the recycle gas flow is dried $P_{O_2} \gg P_{H_2O}$ we end up with the approximation:

$$1 \approx \frac{[Z]}{[Z^0]}\left(1 + \left(P_{O_2}K_1\right)^{1/2}\left(1 + P_{CH_4}K_2\right)\right) \qquad \text{eq. SI-4\_6}$$

Introducing fractional coverages θ_Z , θ_{ZO} , θ_{ZOHCH3} , θ_{ZOH} for $\frac{[Z]}{[Z^0]}$, $\frac{[ZO]}{[Z^0]}$, $\frac{[ZOHCH3]}{[Z^0]}$, $\frac{[ZOH]}{[Z^0]}$, respectively, we get :

$$\theta_Z = \left(1 + \left(P_{O_2}K_1\right)^{1/2}\left(1 + P_{CH_4}K_2\right)\right)^{-1} \qquad \text{eq. SI-4\_7}$$

$$\theta_{ZO} = \theta_Z\left(P_{O_2}K_1\right)^{1/2} \qquad \text{eq. SI-4\_8}$$

$$\theta_{ZOHCH3} = \theta_Z\theta_{ZO}P_{CH_4}K_2 \qquad \text{eq. SI-4\_9}$$

$$\theta_{ZOH} = \left(\theta_Z \theta_{ZO} \frac{P_{H_2O}}{K_9}\right)^{1/2} \qquad \text{eq. SI-4\_10}$$

Next, we further assume: i) that forward step 2, the entrance channel for carbonaceous species to the adsorbed state at the catalyst surface is the overall limiting step; ii) that the comparatively very fast reaction rates for forward steps 3 to 8 are of first order with respect to the respective reacting species. It follows that fractional coverages by other carbonaceous species than ZOHCH3 remain always small fractions of θ_{ZOHCH3} which can be considered as a bundled coverage by carbon in the competition for available surface sites. Denoting k_i the rate constant for step i, and since the rates of consecutive reverse steps 3, 4 and 6 are considered negligible before the corresponding forward rates, we obtain from simple material balances:

$$\theta_{ZOHCH2} = \frac{k_2}{k_4}\theta_{ZOHCH3} \qquad \text{eq. SI-4\_11}$$

$$\theta_{ZOHCH2O} = \frac{k_2 \theta_{ZO} \theta_{ZOHCH3}}{(k_5 + k_6 \theta_{ZO})} \qquad \text{eq. SI-4\_12}$$

$$\theta_{ZHCOOH} = \frac{k_2 k_6 {\theta_{ZO}}^2 \theta_{ZOHCH3}}{(k_5 + k_6 \theta_{ZO})(k_7 + k_8 \theta_{ZO})} \qquad \text{eq. SI-4\_13}$$

And therefore the rates of production of the final gaseous products of methane oxidation CH_2O, CO and CO_2:

$$w_{CH_2O} = k_5 \theta_{ZOHCH2O} = \frac{k_5 k_2 \theta_{ZO} \theta_{ZOHCH3}}{(k_5 + k_6 \theta_{ZO})} \qquad \text{eq. SI-4\_14}$$

$$w_{CO} = k_7 \theta_{ZHCOOH} = \frac{k_7 k_2 k_6 {\theta_{ZO}}^2 \theta_{ZOHCH3}}{(k_5 + k_6 \theta_{ZO})(k_7 + k_8 \theta_{ZO})} \qquad \text{eq. SI-4\_15}$$

$$w_{CO_2} = k_8 \theta_{ZO} \theta_{ZHCOOH} = \frac{k_2 k_6 k_8 {\theta_{ZO}}^3 \theta_{ZOHCH3}}{(k_5 + k_6 \theta_{ZO})(k_7 + k_8 \theta_{ZO})} \qquad \text{eq. SI-4\_16}$$

While the total rate of methane oxidation is:

$$w_{CH_4} = k_2 \theta_{ZOHCH3} \qquad \text{eq. SI-4\_17}$$

The selectivity towards formation of a given product is determined by the ratio of its formation to the overall rate of reaction. Dividing equations SI-4_14 to SI-4_16 by equation SI-4_17 we obtain the adequate fractional selectivities (summing up to 1):

$$S_{CH_2O} = \frac{k_5}{(k_5+k_6\theta_{ZO})} \qquad \text{eq. SI-4\_18}$$

$$S_{CO} = \frac{k_7 k_6 \theta_{ZO}}{(k_5+k_6\theta_{ZO})(k_7+k_8\theta_{ZO})} \qquad \text{eq. SI-4\_19}$$

$$S_{CO_2} = \frac{k_6 k_8 {\theta_{ZO}}^2}{(k_5+k_6\theta_{ZO})(k_7+k_8\theta_{ZO})} \qquad \text{eq. SI-4\_20}$$

Equilibrium adsorption constants from gas phase $K_{i,j}$ for components i =1, 2 and 9, (i.e. O_2, CH_4 and H_2O respectively) and may be expressed as functions of standard pressures P_i^0 and standard free enthalpies of adsorption $\Delta G_{i,j}^0(T)$, where subscript j accounts for the specificity of a given catalytic surface:

$$K_{i,j} = \frac{1}{P_i^0} exp\left(\frac{-\Delta G_{i,j}^0(T)}{RT}\right) \qquad \text{eq. SI-4\_21}$$

Rate constants $k_{l,j}$, where subscript l = 2,5,6,7,8 relates to the forward step number, and subscript j to the catalyst as above, can be expressed according to Eyring:

$$k_{l,j} = \frac{k_B T}{h} exp\left(\frac{-\Delta G_{l,j}^{\pm}(T)}{RT}\right) \qquad \text{eq. SI-4\_22}$$

Where k_B and h are the Boltzmann and Planck constants respectively, and $\Delta G_{l,j}^{\pm}(T)$ is the free energy of activation of step l for catalyst j.

In order to test the ability of this kinetic model to predict the patterns of activity and selectivities obtained from our methane oxidation experiments catalyzed by the set of 12 solid phosphates described in the present report, the next step was to introduce quantitative dependencies of free energies $\Delta G_{i,j}^0(T)$ and $\Delta G_{l,j}^{\pm}(T)$ with respect to numerical descriptors of

the catalysts. For the latter, the natural choice was bond energies $E_{MO,j}$ and $E_{POa,j}$ computed by DFT, and experimental total acidities H_j^0 as presented and tabulated in the main text.

Decomposing free energies of adsorption and activation into their entropic $\Delta S_{i,j}^0$ $\Delta S_{l,j}^{\pm}$, and enthalpic $\Delta H_{i,j}^0$, $\Delta H_{l,j}^{\pm}$ components assumed temperature independent, we postulate linear continuous relationships between enthalpies and bond energies:

$$\Delta H_i^0 = E_i^0 - \beta_i E_{XO} \qquad \text{eq. SI-4\_23}$$

$$\Delta H_l^{\pm} = E_l^{\pm} - \alpha_l E_{XO} \qquad \text{eq. SI-4\_24}$$

Where E_{XO} is the bond energy, and in our case X=M or X=P, since we consider M and P cations at the surface as contributing potential sites. Energies E_i^0, $E_l^{\pm}$ and adimensional coefficients β_i, α_l are parameters to be determined in the fitting protocol described below. Equations SI-4_23 are usually referred to as compensation relationships, and equations SI-4_24 as Brönsted-Evans-Polanyi (BEP) relationships.

The selectivity in formaldehyde is, according to this model, crucially determined by the competition between forward steps 5 and 6. Forward step 5 is the desorption of CH_2O from the Z center of a ZOH site, as pictured below by Fig. SI-5-3, therefore breaking a Z-C bond. CH_2O is a very polar molecule, and in the adsorbed state its carbonyl group will undergo an electrophilic attack of the terminal oxygen by any vicinal acidic proton (e.g. $H^{\delta+}\ldots O^{\delta-}$=P) and a nucleophilic attack of the carbon by the conjugated base (e.g. O^-=P), thus weakening the Z-CH_2O bond. Therefore, the more acidic the catalyst, the easier the desorption of formaldehyde and this explains why the total acidity H^0 can be taken as a proximal descriptor of Z-CH_2O bonds weaknesses. By analogy with BEP relationships like equations SI-4_24, we introduce for forward step 5:

$$\Delta H_5^{\pm} = E_5^{\pm} - \alpha_5 H^0 \qquad \text{eq. SI-4\_25}$$

Where α_5 is positive and has the appropriate dimension $kJ.m^2.\mu mol^{-2}$.

Combining equations S-4_7 to S-4_25, we note that the oxidation rate w_{CH_4} and selectivities in the three gaseous carbonaceous products are completely determined by parameters $\Delta S_{i,j}^0$, $\Delta S_{l,j}^{\pm}$, E_i^0, $E_l^{\pm}$, β_i, α_l, for i = 1, 2 and l = 2, 5, 6, 7, 8 as long as catalysts can be described by E_{XO}, for $X = P, M,$ and H^0. We further assume:

$$\Delta S_{i,j}^0 = \Delta S_i^0 \qquad \text{eq. SI-4\_26}$$

$$\Delta S_{l,j}^{\pm} = \Delta S^{\pm} \qquad \text{eq. SI-4\_27}$$

and in order to express the expected increasing affinity of O_2 for Z sites and decreased affinity of CH_4 for ZO sites as E_{XO} increases, we set $\beta_1 = -1$ and $\beta_2 = 1$.

Therefore 15 parameters remain to be determined through a fitting procedure: ΔS_1^0, ΔS_2^0, E_1^0, E_2^0, $\Delta S^{\pm}$, $E_l^{\pm}$ and α_l for l = 2, 5, 6, 7, 8.

Since we consider X=M and X=P separately, we sum up predicted rates for both kinds of sites and add moreover a catalyst independent thermal rate:

$$w_{CH_4} = W_{CH_4}^M + W_{CH_4}^P + W_{CH_4}^{Th} = k_2^M \theta_{MOHCH3} + k_2^P \theta_{POHCH3} + W_{CH_4}^{Th} \qquad \text{eq. SI-4\_28}$$

where the superscripts M and P refer to the choice of descriptors E_{MO} or E_{PO} in equations SI-4_23 and SI-4_24. The thermal rate, a 16th free parameter, sets a lower limit to the rate in absence of catalyst, and imparts more physical realism by allowing a smooth convergence of the predicted residual rate for vanishing or very high values of the descriptors E_{MO} or E_{PO}. Accordingly, predicted selectivities become:

$$S_A = \frac{w_{CH_4}^M}{W_{CH_4}} S_A^M + \frac{w_{CH_4}^P}{W_{CH_4}} S_A^P \qquad \text{eq. SI-4\_29}$$

For $A = CH_2O, CO, CO_2$

We have adopted a two steps fitting procedure. In the first step an objective function is defined as the root mean square deviation (rmsd) of predicted from experimental Neperian logarithms

of the rates of oxidation w_{CH_4}. This first function is minimized with respect to the eight first parameters ΔS_1^0 , ΔS_2^0 , E_1^0, E_2^0, $\Delta S^{\pm}$, $E_l^{\pm}$ and α_l for $l = 2$, and $W_{CH_4}^{Th}$, using 8 experimental rates of oxidation corresponding to $Mn_2P_2O_7$ and the 7 orthophosphates catalysts (see Table SI-3-3) and constraining $E_2^{\pm}$ to remain positive in the range of E_{XO} values spanned by these catalysts. The four remaining pyrophosphates are excluded from this first training set since they appear obviously out of the regular volcano trend observed, when plotting experimental w_{CH_4} versus E_{XO} . We obtained for this step a relative rmsd of 6.3 %.

In the second step, a second objective function is built as the root mean square deviation of predicted from experimental selectivities, and minimized with respect to the 8 remaining parameters $E_l^{\pm}$ and α_l for l = 5, 6, 7, 8 using all 24 independent experimental selectivities available (see Table S-3-3), constraining $E_l^{\pm}$ for l = 5, 6, 7, 8 to remain positive in the range of E_{XO} values spanned by these catalysts. We obtained for this step a relative rmsd of 1.8 %.

Rate constants given by equation SI-4_17 are converted from theoretical units of molecule.site^{-1}.s^{-1} into experimental units of 10^9 mol.m^{-2}.s^{-1} using an average site density of 1,25.10^{19} m^{-2} estimated according to the volumic density of P atoms reported in Table 1 of main text.

Best fitted parameters are listed in the following Table SI-4-1:

Table SI-4-1: Best fitted parameters of the kinetic model. Other inputs are operating conditions, average site density for phosphate catalysts 1.25 10^{19} site.m^{-2}; T = 873 K, [CH_4]= 10^{-2} mol.l^{-1}; [O_2]= 5.10^{-3} mol.l^{-1} and Boltzmann and Planck fundamental constants k_B and h

ΔS_1^0	73.5	J.mol^{-1}.K^{-1}
ΔS_2^0	201.04	J.mol^{-1}.K^{-1}
$\Delta S^{\pm}$	-56.78	J.mol^{-1}.K^{-1}
E_1^0	0.00	kJ.mol^{-1}
E_2^0	29.96	kJ.mol^{-1}
$E_2^{\pm}$	179.12	kJ.mol^{-1}
α_2	-0.16	-
$E_5^{\pm}$	4.29	kJ.mol^{-1}
α_5	0.32	kJ.m^2.µmol^{-2}
$E_6^{\pm}$	15.62	kJ.mol^{-1}
α_6	-0.04	-
$E_7^{\pm}$	52.21	kJ.mol^{-1}
α_7	-0.29	-
$E_8^{\pm}$	28.98	kJ.mol^{-1}
α_8	-0.36	-
$W_{CH_4}^{Th}$	2.00	10^9.mol.m^{-2}.s^{-1}

SI-5 Molecular models of key surface intermediates along the catalytic pathways

The atomistic models presented in this section were built with the MAPS platform from SCIENOMICS (http://www.scienomics.com) provided to HT and LRS according to their participation to the Scienomics Group of Scientific Excellence (SGSE). The configurations shown were not optimized.

Figure SI-5-1: atomistic model of ZOHCH3 surface species produced from step 2, in the case of a tri-periodic 2 layers slab of SnP_2O_7 exposing two (200) surfaces (the z axis is parallel to the original 200 vector of the SnP_2O_7 Pa-3 cubic unit-cell). The "bottom" surface is fully covered by ≡P-OH and ≡M-OH hydroxyl groups. The "top" surface shows arrays of HO-Sn-CH_3 surface species (noted ≡M(CH_3)-OH), PO species (i.e. ZO with Z=P, noted ≡P=O) and coordinatively unsaturated surface Sn cations (i.e. Z with Z=Sn, noted ≡M). Sn centers in blue, P in magenta, O in red, Carbon in grey, Hydrogen in white. Perspective view.

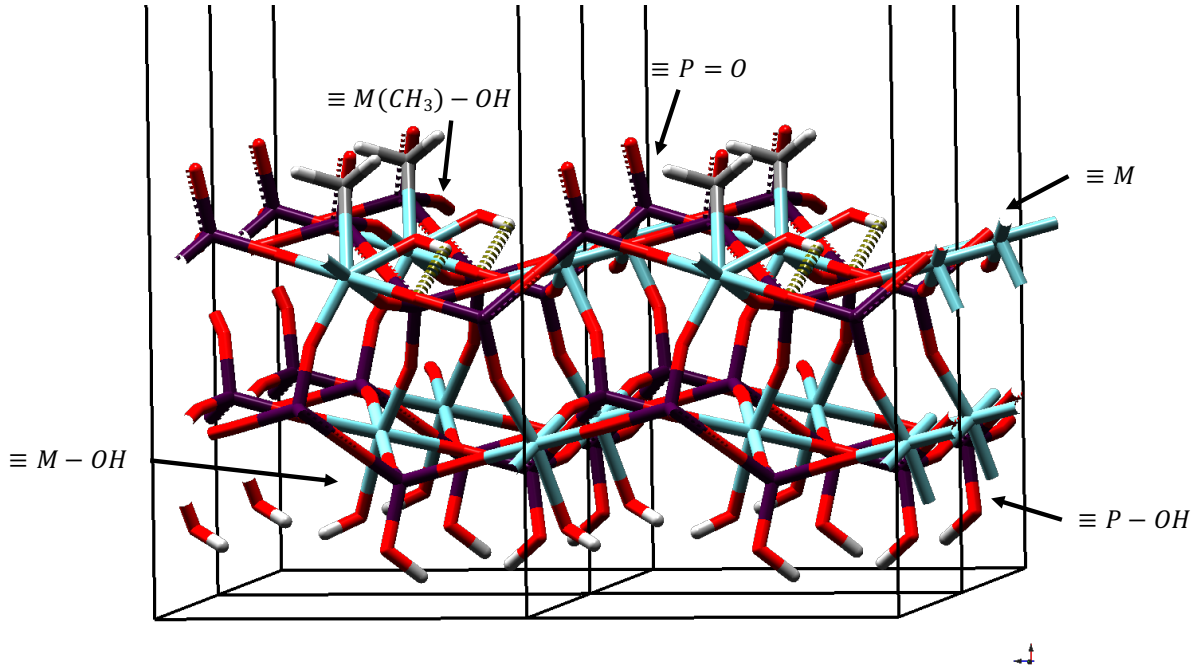

Figure SI-5-2: atomistic model of ZOHCH2 surface species produced from step 3, in the case of a tri-periodic 2 layers slab of SnP_2O_7 exposing two (200) surfaces (the z axis is parallel to the original 200 vector of the SnP_2O_7 Pa-3 cubic unit-cell). The "bottom" surface is fully covered by ≡P-OH and ≡M-OH hydroxyl groups. The "top" surface shows arrays of HO-Sn-CH_2 surface species (noted ≡M(CH_2)-OH), P-OH species (i.e. ZOH with Z=P, noted ≡P-OH) and Sn-OH species (i.e. ZOH with Z=Sn, noted ≡M-OH). Sn centers in blue, P in magenta, O in red, Carbon in grey, Hydrogen in white. Perspective view.

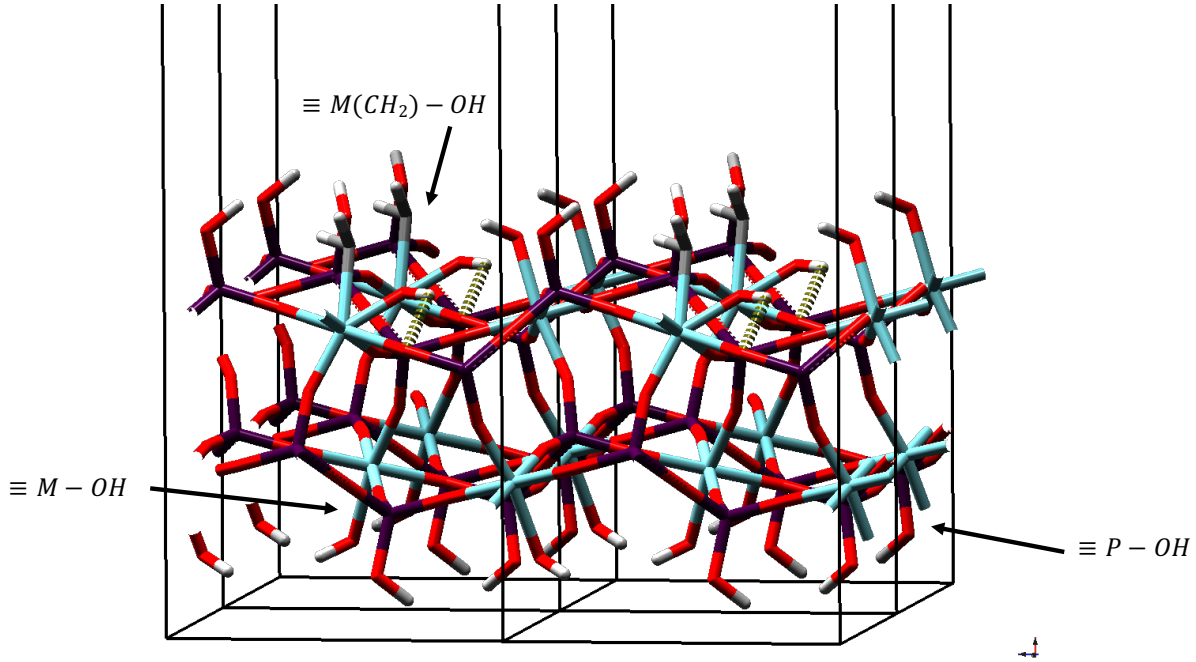

Figure SI-5-3: atomistic model of ZOHCH2O surface species produced from step 6 in the case of a tri-periodic 2 layers slab of SnP_2O_7 exposing two (200) surfaces (the z axis is parallel to the original 200 vector of the SnP_2O_7 Pa-3 cubic unit-cell). The "bottom" surface is fully covered by ≡P-OH and ≡M-OH hydroxyl groups. The "top" surface shows arrays of HO-Sn-CH_2O surface species (noted ≡M(O=CH_2)-OH), POH species (i.e. ZOH with Z=P, noted ≡P-OH) and coordinatively unsaturated surface Sn cations (i.e. Z with Z=Sn, noted ≡M). Sn centers in blue, P in magenta, O in red, Carbon in grey, Hydrogen in white. Perspective view.

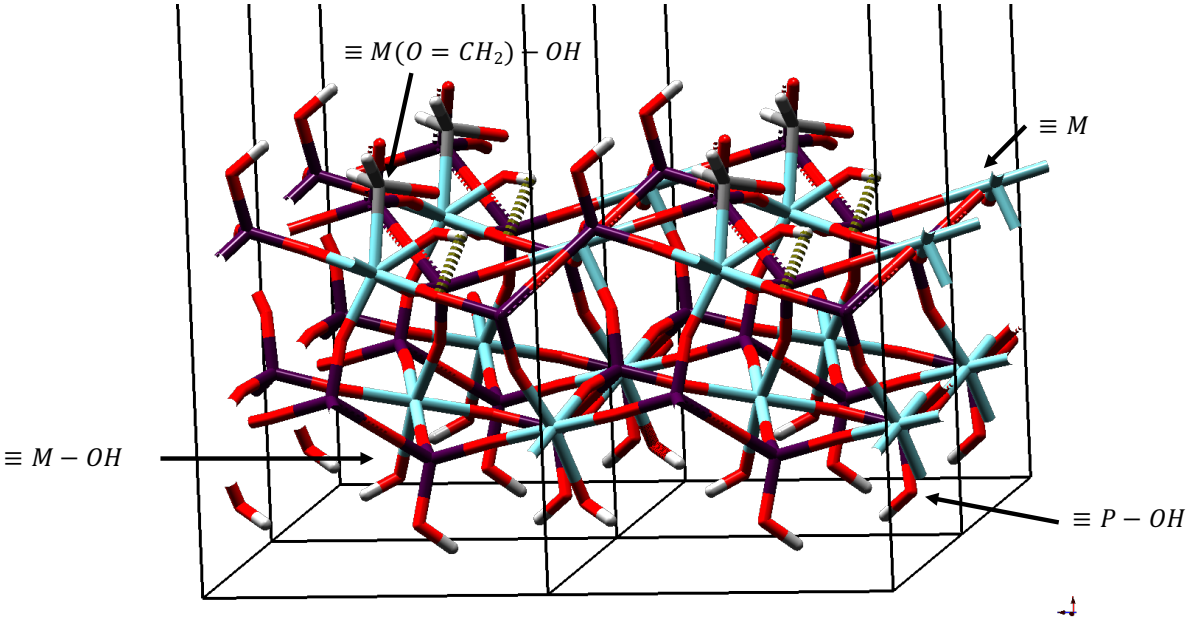

Figure SI-5-4: atomistic model of ZHCOOH surface species produced from step 6 in the case of a tri-periodic 2 layers slab of SnP_2O_7 exposing two (200) surfaces (the z axis is parallel to the original 200 vector of the SnP_2O_7 Pa-3 cubic unit-cell). The "bottom" surface is fully covered by ≡P-OH and ≡M-OH hydroxyl groups. The "top" surface shows arrays of Sn-HCOOH surface species (noted ≡M(HCOOH), POH species (i.e. ZOH with Z=P, noted ≡P-OH) and coordinatively unsaturated surface Sn cations (i.e. Z with Z=Sn, noted ≡M). Sn centers in blue, P in magenta, O in red, Carbon in grey, Hydrogen in white. Perspective view.